

1 **Measurement report: Long-term measurements of aerosol precursor concentrations in the Finnish sub-  
2 Arctic boreal forest**

3 Tuija Jokinen<sup>1,2\*</sup>, Katrianne Lehtipalo<sup>1,3</sup>, Roseline Cutting Thakur<sup>1</sup>, Ilona Ylivinkka<sup>1</sup>, Kimmo Neitola<sup>1</sup>, Nina  
4 Sarnela<sup>1</sup>, Totti Laitinen<sup>1</sup>, Markku Kulmala<sup>1</sup>, Tuukka Petäjä<sup>1</sup> and Mikko Sipilä<sup>1</sup>

5 <sup>1</sup>Institute for Atmospheric and Earth System Research (INAR) / Physics, Faculty of Science, University of  
6 Helsinki, P.O. Box 64, Helsinki, 00014 University of Helsinki

7 <sup>2</sup>Climate & Atmosphere Research Centre (CARE-C), The Cyprus Institute, P.O. Box 27456, Nicosia, CY-  
8 1645, Cyprus

9 <sup>3</sup>Finnish Meteorological Institute, Helsinki, Finland

10 \*correspondence to [t.jokinen@cyi.ac.cy](mailto:t.jokinen@cyi.ac.cy)

11

12 **Abstract:**

13 Aerosol particles form in the atmosphere by clustering of certain atmospheric vapors. After growing to larger  
14 particles by condensation of low volatile gases, they can affect the Earth's climate by scattering light and by  
15 acting as cloud condensation nuclei. [\(CCN\)](#). Observations of low-volatility aerosol precursor gases have been  
16 reported around the world but longer-term measurement series and any Arctic data sets showing seasonal  
17 variation are close to non-existent. In here, we present ~7 months of aerosol precursor gas measurements  
18 performed with the nitrate based chemical ionization mass spectrometer (CI-APi-TOF). We deployed our  
19 measurements ~150 km North of the Arctic Circle at the continental Finnish sub-Arctic field station, SMEAR  
20 I, [\(Station for Measuring Ecosystem – Atmosphere Relations\)](#), located in Värrö strict nature reserve. We report  
21 concentration measurements of the most common new particle formation [\(NPF\)](#) related compounds; sulfuric  
22 acid (SA), methane sulfonic acid (MSA), iodine acid (IA) and a total concentration of highly oxygenated organic  
23 [compoundsmolecules](#) (HOMs). At this remote measurement site, SA is originated both from anthropogenic  
24 and biological sources and has a clear diurnal cycle but no significant seasonal variation. MSA shows a more  
25 distinct seasonal cycle with concentrations peaking in the summer. Of the measured compounds, [iodine acidIA](#)  
26 concentrations are the most stable throughout the measurement period, except in April, when the concentration  
27 of IA is significantly higher than during the rest of the year. Otherwise, IA has almost identical daily maximum  
28 concentrations in spring, summer and autumn, and on [new particle formationNPF](#) event or non-event days.  
29 HOMs are abundant during the summer months and low in the autumn months. Due to the low autumn  
30 concentrations and their high correlation with ambient air temperature, we suggest that most of HOMs are  
31 products of biogenic emissions, most probably monoterpene oxidation products. [New particle formationNPF](#)  
32 events at SMEAR I happen under relatively low temperatures (1 – 8 °C) with a fast temperature rise in the  
33 early morning hours, lower and decreasing [relative humidity \(RH-\)](#) (55% vs. 80%) during the NPF days  
34 compared to non-event days. NPF days have clearly higher global irradiance values (~450 m<sup>-2</sup> vs. ~200 m<sup>-2</sup>)  
35 and about 10 ppbv higher ozone concentrations than non-event days. During NPF days, we have on average  
36 higher SA concentration peaking at noon, higher MSA concentrations in the afternoon and slightly higher IA  
37 concentration than during non-event days. All together, these are the first long term measurements of aerosol  
38 forming vapors from the SMEAR I in the sub-arctic region, and the results help us to understand atmospheric  
39 chemical processes and aerosol formation in the rapidly changing Arctic.

40 **1. Introduction:**

41 The climate of sub-Arctic region is characterized with some of the most extreme temperature variations on  
42 Earth. We expect that during the course of the 21<sup>st</sup> century, the boreal forest is to experience the largest increase  
43 in temperatures of all forest biomes (IPCC, 2013), making it the most vulnerable to climate change. The boreal  
44 forest (taiga) covers most of the sub-Arctic and encompasses more than 30% of all forests on Earth, being one  
45 of the largest biome in the world (Brandt et al., 2013). The expected rate of changes, may overwhelm the

46 resilience of forest ecosystems and possibly lead to significant biome-level changes (Reyer et al., 2015). The  
47 forest-atmosphere systems are closely interlinked to one another. The forest stores carbon and water in the  
48 peat, soil and as biomass while at the same time vegetation emits volatile organic compounds (VOC) into the  
49 atmosphere (Bradshaw and Warkentin, 2015). In the Arctic, summer is short, but solar radiation is abundant  
50 and extends the daylight hours all the way to midnight and beyond. On the other hand, during the polar night  
51 air pollutants accumulate in the atmosphere due to cold and stable atmosphere, while turbulent mixing is  
52 inhibited, and the lack of removal processes lead to the formation of Arctic haze (Stohl, 2006). These features  
53 make the Arctic an interesting study region for photochemistry of reduced atmospheric compounds. Oxidation  
54 processes that dominantly occur in the summer time control the processes removing VOCs and other traces  
55 gases, such as  $\text{SO}_2$  and  $\text{NO}_x$ , from the atmosphere in the Arctic. Detailed understanding of atmospheric  
56 processes leading to aerosol precursor formation and gas-to-particle conversion and their role in feedback  
57 mechanisms help in assessing the future climate.

58 Aerosol and trace gas measurements in the sub-Arctic field station SMEAR I, go back to the 90s (Ahonen et  
59 al., 1997; Kulmala et al., 1998; Mäkelä et al., 1997). Trace gas and aerosol measurements at SMEAR I started  
60 in 1992 making them one of the longest continuous measurements of aerosol particle number and size  
61 distributions in the sub-Arctic (Ruuskanen et al., 2003). These long-term measurements show that aerosol  
62 particles regularly form and grow from very small sizes (< 8 nm diameter) with the highest frequency in the  
63 spring, between March and May (Dal Maso et al., 2007; Vehkamäki et al., 2004). It is suggested, that spring  
64 promotes new particle formation (NPF) because of the awakening of biological processes after the winter. At  
65 SMEAR I the snow only melts away in May-June and thus, many biological processes (photosynthesis)  
66 activate while the snow is still deep. This makes the Arctic spring a very complex environment for atmospheric  
67 chemistry with possible emission sources from melting snow, ice, melt water, vegetation and transport from  
68 other areas. At SMEAR I, most of the observed NPF events are either connected to clean air arriving from the  
69 Northern sector (originating from The Arctic Ocean and transported over boreal forest, Dal Maso et al., 2007)  
70 or the polluted air masses from the Eastern sector (Kyrö et al., 2014; Sipilä et al., 2021). Annually, around 30-  
71 60 NPF events are recorded at SMEAR I, of which around half could be initiated by anthropogenic air  
72 pollutants from the Kola Peninsula (Kyrö et al., 2014; Pirjola et al., 1998; Sipilä et al., 2021) leaving half of  
73 the events occurring from natural sources. The trend of NPF occurrence in Väriö is decreasing, as the  
74 anthropogenic sulfur dioxide emissions are decreasing in Russia (Kyrö et al., 2014).

75 Formation and growth of new particles at SMEAR I usually happen during daylight, highlighting the  
76 importance of photochemical activities. However, unlike most other locations, NPF is also observed during  
77 nighttime or polar night (Kyrö et al., 2014; Vehkamäki et al., 2004). Formation and growth processes of  
78 aerosols seem not to be correlated with each other at SMEAR I (Vehkamäki et al., 2004). Earlier literature  
79 reports, that the formation rate ( $J$ ) has no clear seasonal trend, while the growth rates (GR) of small particles  
80 clearly peak during summer (Ruuskanen et al., 2007). This indicates that different chemistry drives the initial  
81 cluster formation and the subsequent growth processes. From the observed nucleation rates it has been  
82 proposed that NPF at SMEAR I could be due to sulfuric acid~~SA~~ –ammonia (-water) nucleation (Napari et al.,  
83 2002) likely dominated by ion-induced channel at least during winter months (Sipilä et al., 2021). Kyrö et al.,  
84 (2014) concludes that 20-50% of the condensational growth can also be explained by sulfuric acid~~SA~~ in Väriö.  
85 Other studies speculate about the possibility of different organic compounds participating in NPF in the sub-  
86 Arctic. Tunved et al., (2006) studied the air masses arriving to SMEAR I and concluded that the aerosol mass  
87 increased linearly with time that the air masses travelled over land. The concentration of condensing gases  
88 over the boreal forest was concluded to be high and most likely consisting mainly of oxidation products of  
89 terpenes (VOCs) that are emitted by the forest. At SMEAR II station in Hyytiälä, approximately 700 km South-  
90 West of Väriö, oxidized organics mostly explain the growth of newly formed particles (Bianchi et al., 2017;  
91 Ehn et al., 2014). However, direct measurements of the aerosol forming and growing vapor species are still  
92 lacking from SMEAR I except during wintertime without biogenic activity when sulfuric acid~~SA~~ has been  
93 shown to be primarily responsible on formation and growth (Sipilä et al., 2021). In Väriö, the role of NPF is  
94 critical in forming of cloud condensation nuclei (CCN), since measurements show that the number of  
95 CCN can increase up to 800 % as a result of NPF (Kerminen et al., 2012). In other locations in the boreal forest

96 and Arctic, some measurements shed light into the possible chemical components that could be forming  
97 particles in Väriö. Currently, the closest continuous measurements with the nitrate based CI-APi-TOF are  
98 conducted in Hytylä at the SMEAR II-station (Jokinen et al., 2012, 2017; Kulmala et al., 2013). In Hytylä  
99 there is direct evidence on the key role of the photochemical production of sulfuric acidSA and HOMs  
100 maintaining atmospheric NPF (Bianchi et al., 2017; Ehn et al., 2014; Jokinen et al., 2017; Kulmala et al.,  
101 2013).

102 Other chemical composition measurements of aerosol precursors have been conducted only in a few locations  
103 in the High-Arctic and over the Arctic Ocean (Baccarini et al., 2020; Beck et al., 2021; He et al., 2021; Sipilä  
104 et al., 2016). These studies show that in the Arctic, the marginal ice zone and the coast of the Arctic Ocean is  
105 a source of atmospheric iodic acidIA that is efficiently forming new particles. Sulfuric acidSA and MSA  
106 concentrations were also reported (Beck et al., 2021), but they were much lower in concentration than iodic  
107 acidIA (Baccarini et al., 2020). However, the chemistry behind NPF is not that simple, even in the pristine  
108 Arctic air. The clean air above the Arctic Ocean is abundant in dimethyl sulfide (DMS) emitted by  
109 phytoplankton, that rapidly oxidizes into sulfuric acidSA and MSA on sunny days and consequently forms  
110 cloud condensation nucleiCCN (Charlson et al., 1987; Park et al., 2018). Beck et al., (2021) report, that in  
111 Svalbard in the Arctic Ocean, sulfuric acidSA and methane sulfonic acidMSA contribute to the formation of  
112 secondary aerosol. They also observed that these compounds formed particles large enough to contribute to  
113 some extent to cloud condensation nuclei(CCN)CCN. This is supported by measurements of aerosol chemical  
114 composition from the Arctic that commonly report MSA in particulate matter (Dall Osto et al., 2018; Kermanen  
115 et al., 1997). According to Beck et al. (2021) the initial aerosol formation in the high Arctic occurs via ion-  
116 induced nucleation of sulfuric acidSA and ammonia and subsequent growth by mainly sulfuric acidSA and  
117 MSA condensation during springtime and highly oxygenated organic molecules (HOM) during summertime.  
118 By contrast, in an ice-covered region around Villum, Greenland, Beck et al. (2021) observed new particle  
119 formationNPF driven by iodic acidIA, but the particles remained small and did not grow to CCN sizes due to  
120 insufficient concentration of condensing vapors. Since the Arctic CCN number concentrations are low in  
121 general, formation of new particles is a very sensitive process affecting the composition of the aerosol  
122 population and CCN numbers in the area.

123 In this article, we present the measurements of aerosol precursor molecules from the continental SMEAR I  
124 station, ~150 km North of the Arctic Circle and ~150 km from the Arctic Ocean. We measured sulfuric acid,  
125 methane sulfonic acid, iodic acidSA, MSA, IA and highly oxygenated organic compoundHOM concentrations  
126 with a sulfuric acidSA calibrated CI-APi-TOF (Jokinen et al., 2012; Kürten et al., 2012) to determine their  
127 levels in the sub-Arctic boreal forest and to understand whether these species are connected with the aerosol  
128 formation process in the area.

## 129 2. Methods, measurement site and instrumentation:

130 The core of this work is measurements of gas phase aerosol precursors. We use the nitrate chemical ionization  
131 atmospheric pressure interface time-of-flight mass spectrometer (CI-APi-ToF) that has been operational at the  
132 SMEAR I-station (N67°46, E29°36) in Eastern-Lapland since the early spring of 2019. SMEAR stands for  
133 Station for Measuring Ecosystem – Atmosphere Relations. Measurements were done on top of Kotovaara hill  
134 (390 m a.s.l.), close to ground level in an air-conditioned small log wood cottage. The cottage is surrounded  
135 by ~65-year-old Scots pine forest. More details about the station can be found in earlier publications (Hari et  
136 al., 1994; Kyrö et al., 2014). The mass spectrometric measurements are designed to start a long-term  
137 measurement series of atmospheric aerosol forming trace gases in the Finnish Lapland and the measurements  
138 are ongoing to this day. We measure e.g. sulfuric acid, iodic acid, highly oxygenated organic molecules and  
139 methane sulfonic acidSA, IA, HOMs and MSA with high time resolution and precision. The measurements  
140 are running in Finnish winter time (UTC+2) throughout the year.

141 We calibrated the CI-APi-TOF twice during the measurement period and run the instrument with the same  
142 settings for the whole measurement period reported in this paper. We calibrated the instrument using a sulfuric  
143 acidSA calibrator described in Kürten et al., (2012.). The calibration factor from the two separate calibrations

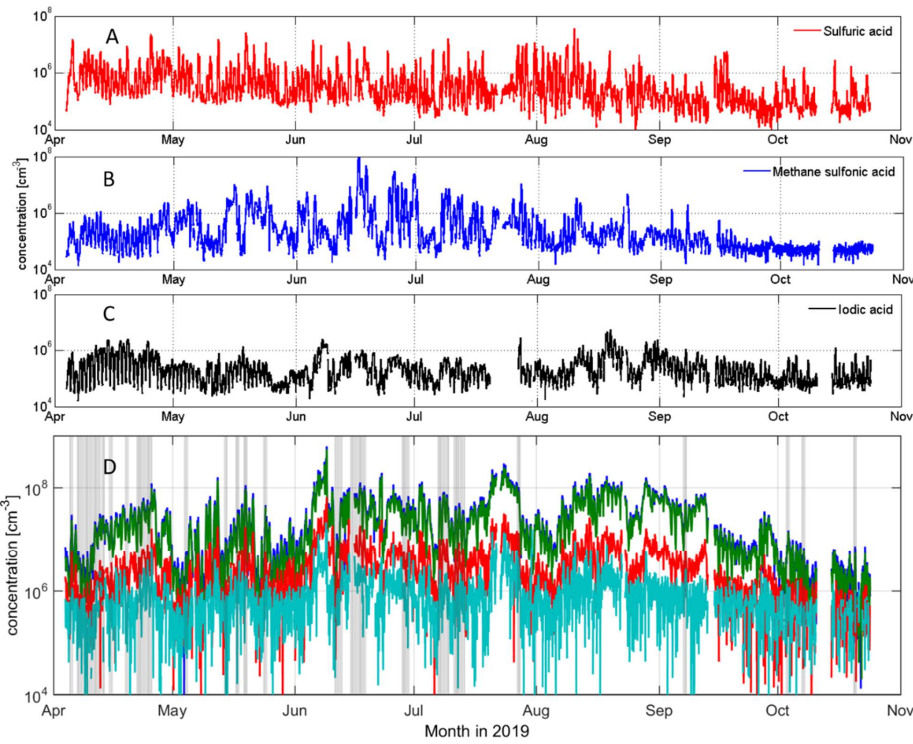
were 1)  $7 \cdot 10^9$  and 2)  $8 \cdot 10^9$  and we use the average  $7.5 \cdot 10^9$  in our study calculate the concentrations of all reported compounds. This factor includes the loss parameter due to the  $\sim 1$  m long unheated inlet tube (3/4" stainless steel). HOMs and ~~iodic-acid~~**IA** have been estimated to be charged similarly at the kinetic limit as ~~sulfuric-acid~~**SA** (Ehn et al., 2014; Sipilä et al., 2016), so the calibration factor for them should be similar, but please note, that the concentration of other compounds than SA can be highly uncertain due to different ionizing efficiencies, sensitivities and other unknown uncertainties. If MSA, IA or HOMs do not ionize at the kinetic limit these concentrations could be underestimated and thus, the concentrations reported in here should be taken as low limit values. The ~~sulfuric-acid, iodic-acid~~**SA, IA** and MSA data presented in this study are all results of high-resolution peak fitting of the CI-APi-TOF, in order to avoid inaccurate identification of compounds and to separate overlapping peaks. The HOM data is a sum of mass-to-charge ratios from 300 to 400 Th, representing the monomer HOM range ( $C_{10}$  compound range), 401 to 500 Th for the slightly larger HOMs ( $C_{15}$  compound range) and 501 to 600 Th for the dimer species ( $C_{20}$  compound range). We also give the sum of these all (from 300 to 600 Th). The goal of this article is not to specify different HOM compounds or to study NPF in mechanistic details but to give an overview of general seasonal trends and variations of these selected species. Note that since this is a sum of all peaks in the selected mass range, we cannot assure that all the compounds included are HOMs. However, the investigation in laboratory conditions show that the nitrate-Cl-APi-TOF is highly selective and sensitive towards HOMs with  $O > 5$  (Riva et al., 2019) and with hydroperoxide (-OOH) functionalities (Hyttilä et al., 2015). All data obtained from the CI-APi-TOF we analyzed using tofTools program described in (Junninen et al., 2010) and averaged over an hour. The original data time resolution is 5 sec. The uncertainty range of the measured concentrations reported in this study is estimated to be  $-50\% + 100\%$  and the limit of detection,  $LOD \cdot 4 \cdot 10^4$  molecules  $\text{cm}^{-3}$  (Jokinen et al., 2012).

To classify NPF events recorded during the measurement period, we used the data measured by a Differential Mobility Particle Sizer (DMPS). Condensation sink was also calculated using the DMPS data. The DMPS instrument and earlier statistics of NPF events in Värrö has been documented by (Dal Maso et al., 2007; Vana et al., 2016; Vehkamäki et al., 2004). The NPF events were classified according to (Maso et al., 2005). Total aerosol particle number concentration was measured with a Condensation Particle Counter (CPC, TSI 3776) in the size range of 3 – 800 nm. Air ion size distributions were measured with the Neutral cluster and Air Ion Spectrometer, NAIS (Kulmala et al., 2007; Manninen et al., 2016; Mirme and Mirme, 2013) that measures negative and positive ions in the size range of 0.8 – 42 nm in mobility diameter and total particle size distribution between  $\sim 2$  and 42 nm. ~~All meteorological parameters, trace gas concentrations and aerosol data were downloaded directly from smartSMEAR open-access database (<https://smear.avaa.ese.fi/>) and all-mass spectrometric data are available on request.~~

### 3. Results and discussion:

#### 3.1. Overview of the whole measurement period:

You can see a time series of the most common aerosol precursor compounds; ~~sulfuric-acid, methane-sulfonic acid, iodic-acid~~**SA, MSA, IA** and sums of different HOM groups in Figure 1. This figure depicts the whole measurement period from April 4 to October 27 in 2019. Overall, we succeeded to measure the whole 7 month period almost uninterrupted. Only a few short power cuts stopped our measurements during this time. ~~iodic-acid~~**IA** data is missing from late July since its peak could not be separated well enough from overlapping peaks in the spectra during this time. This was due to poor resolution (low signal of  $\text{IO}_3^-$  close to another peak) that makes peak integration to give negative, unreal values and we thus decided to flag them out. After late October, the instrument malfunctioned and stopped our measurements. In this particular article, we present data from spring (Apr-May), summer (Jun-Jul-Aug) and autumn (Sep-Oct) 2019. More about the SMEAR I winter observations can be read in Sipilä et al., 2021 where they report observations of polar night pollution events from Värrö after the CI-APi-TOF was fixed.



189

190 **Figure 1.** Overview of sulfuric (A), methane sulfonic (B) and iodic acid (C), as well as HOM (D)  
 191 concentrations at SMEAR I in April to October 2019. NPF days are depicted in grey shading in panel D. All  
 192 data in panels A-C are resulting from high-resolution peak fitting. HOM data are sums of certain mass ranges;  
 193 from 300 to 400 Th in green, representing C10 or HOM monomer compounds, from 401 to 500 Th in red,  
 194 representing C15 compound and from 501 to 600 Th on light blue, representing C20 or HOM dimer  
 195 compounds. The sum of HOM (darker blue) is a sum of the aforementioned mass ranges. The sum of HOMs  
 196 is approximately one order of magnitude higher than SA, MSA or IA concentrations during this measurement  
 197 period.

198 In Figure 2 we show some of the most interesting environmental and meteorological parameters that influence  
 199 the atmospheric gas composition during the measurements period; temperature, global radiation and snow  
 200 depth, ozone,  $\text{NO}_x$  and  $\text{SO}_2$  mixing ratios. There are some special features in year 2019; the summer had two  
 201 heat waves, when the air temperature rose up to 29.2 °C in early June and to almost the same values in late  
 202 July. These episodes are getting more common in Lapland due to climate change. These warmer conditions  
 203 will probably change the emissions of trace gases including the composition and abundance of aerosol  
 204 precursors in the future Arctic environment (Schmale et al., 2021). However, heat wave conditions are likely  
 205 not favorable conditions to NPF since condensation of low-volatility gases is favored in colder temperatures  
 206 (via the vapor pressure decrease due to lower temperatures), but they may affect the oxidation chemistry of  
 207 VOCs by promoting dimer formation.

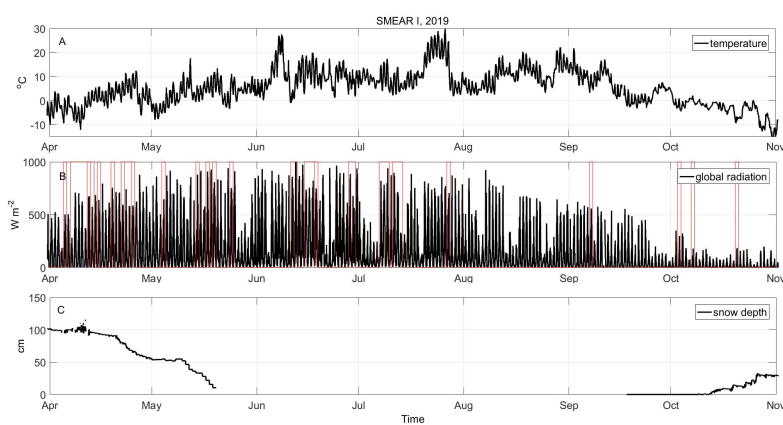
208 From Figure 2, we also see that the snow covered period ended in 2019 in late May and snow started to  
 209 accumulate again in mid-October. Solar radiation (Figure 2A) is intense in Värrö during springtime and gives

210 Värrö favorable photo-oxidizing conditions, effectively removing air pollutants and trace gases from the  
 211 atmosphere. Photochemical activity in presence of NO<sub>x</sub> (Figure 2E), produces ozone in springtime and this is  
 212 visible in very high ozone mixing ratios at the site (Figure 2D). Median ozone mixing ratios were around 55  
 213 ppbv in April and decreased to ~30 ppbv in the late summer and autumn. The spring ozone mixing ratio in  
 214 2019 was significantly higher than the previous reports from the years 1992 to 2001, when monthly mean  
 215 values of ozone varied between 25 – 40 ppbv (Ruuskanen et al., 2003).

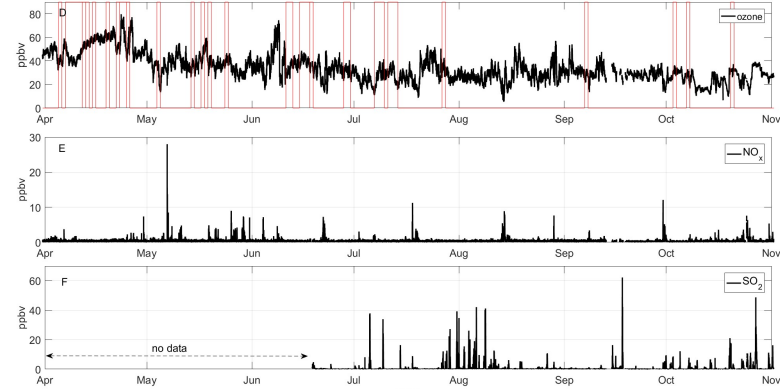
216 The springtime diurnal solar cycle is clearly visible with all studied compounds. All measured aerosol  
 217 precursor compounds are abundant even during the period when snow covers the ground in the spring. The  
 218 HOM concentrations follow the increasing solar radiation and rising temperature. MSA has a stronger diurnal  
 219 cycle before the snow melt than after it. This may be due to rain and cloudy conditions that are more common  
 220 in the summer. *Sulfuric acid*SA and *iodic acid*IA do not have such strong seasonal variation than HOMs and  
 221 MSA. The aerosol precursor concentrations are discussed in more detail in the following sections.

### 222 3.2. Seasonal and monthly variation of SA, MSA, *iodic acid*IA and HOM concentrations

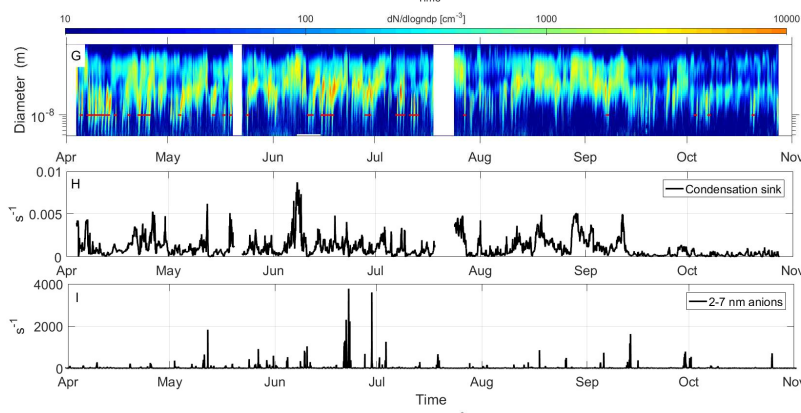
223 We present the diurnal variation of aerosol precursors; *sulfuric acid*, *methane-sulfonic acid*, *iodic acid*SA,  
 224 *MSA*, *IA* and highly oxygenated molecules, concentrations separately for different seasons accompanied with  
 225 solar radiation and total aerosol number concentrations in Figure 3. Strong seasonality is most evident in  
 226 *sulfuric acid*SA and HOM concentrations. SA is at its highest in the spring, decreasing toward summer and  
 227 autumn while HOMs reach their maximum in the summer. We detect an increase in total aerosol number  
 228 concentration on the spring evenings that is likely due to more frequent NPF events taking place at SMEAR I.  
 229 The increase in HOMs in the summer at SMEAR I is linked to the increased emissions of VOCs from  
 230 vegetation that oxidize into HOMs via ozonolysis (Ehn et al., 2014) and OH-radical reactions (Berndt et al.,  
 231 2016; Jokinen et al., 2014, 2017; Wang et al., 2018). The overall lowest aerosol precursor concentrations and  
 232 aerosol number concentration we detect during autumn (winter data was missing from this study, see Sipilä et  
 233 al. 2021, for winter time observations made promptly after the period reported here). MSA shows very similar  
 234 concentrations during spring and summer, and drops down to the limit of detection level for autumn. *iodic*  
 235 *acid*IA acts very differently than the other compounds. We observe *iodic acid*IA to have a similar level of  
 236 concentration throughout the measurement period and seems that the concentration reaches a steady state  
 237 during daylight hours. This daytime maximum stays at the same level about 5 hours longer during spring than  
 238 in the autumn. The day length getting shorter towards the autumn explains this behavior. The maximum hourly  
 239 median concentrations for the measured compounds are  $\sim 2 \cdot 10^6 \text{ cm}^{-3}$  for SA (spring),  $\sim 5 \cdot 10^5 \text{ cm}^{-3}$  for MSA  
 240 (summer),  $\sim 3 \cdot 10^5 \text{ cm}^{-3}$  for *iodic acid*IA (all seasons) and  $\sim 5 \cdot 10^7 \text{ cm}^{-3}$  for the sum of HOMs (summer, mass  
 241 range from 300 to 600 Th).



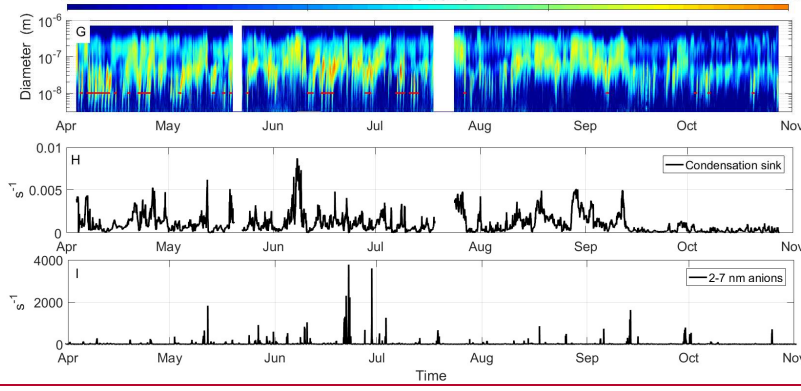
243



244



245



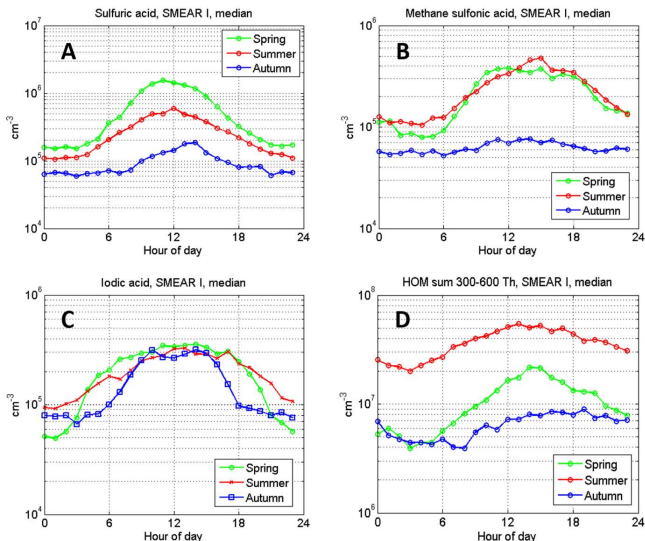
246

247 **Figure 2:** Observations of temperature (A), global radiation (B), snow depth (C), ozone (D), NO<sub>x</sub> (E) and SO<sub>2</sub>  
248 (F) mixing ratios, number size distribution (G), condensation sink (H) and concentration of 2-7 nm anions (I)

249 at SMEAR I during the measurement period. SO<sub>2</sub> data is missing until mid-June due to instrumental  
 250 malfunction. NPF event times are depicted in red in subplots (B), (D) and (G).

251 We can compare these numbers to SMEAR II long-term (5-year median concentration) observations, were the  
 252 median peak SA concentrations are  $\sim 1.5 \cdot 10^6 \text{ cm}^{-3}$ ,  $\sim 1 \cdot 10^6 \text{ cm}^{-3}$  and  $\sim 3 \cdot 10^5 \text{ cm}^{-3}$  for spring, summer and  
 253 autumn, respectively (Sulo et al., 2021). These measured concentrations are very similar to SMEAR I  
 254 observations except a slightly higher summer and autumn SA concentration at SMEAR II. However, it should  
 255 be noted that the springtime measurements from SMEAR I do not include March data, which makes the  
 256 springtime comparison somewhat uncertain. [The SMEAR II data set that includes March data cannot be  
 257 expected to be perfectly comparable with our data](#). However, as reported by Sipilä et al., 2021 the March data  
 258 from the following year seems very similar concentration levels what we report in here for spring (max.  $\sim 2 \cdot 10^6$   
 259  $\text{cm}^{-3}$  and daily averages peak around  $0.5 \cdot 10^6 \text{ cm}^{-3}$ ). We expect that the SA concentrations are only marginally  
 260 affected by the lack of March data, but that the level of HOMs or MSA or IA could be affected more due to  
 261 very different meteorological conditions between the stations in springtime (SMEAR II is  $\sim 700$  km more South  
 262 than SMEAR I). There is also a difference in the timing of the peak SA concentration in the summer. At  
 263 SMEAR I the peak concentration is reached at noon and at SMEAR II it can be found some hours earlier,  
 264 already around eight o'clock in the morning (Sulo et al., 2021). In the case of HOMs, we cannot compare the  
 265 concentrations directly to Sulo et al. (2021) as they calculated the sum of HOMs differently, only taking into  
 266 account the most abundant signals and separating nitrate and non-nitrate HOMs. However, we take the liberty  
 267 to compare diurnal and seasonal variations. Both at SMEAR I and II, observations show the highest HOM  
 268 concentrations during summer, while the autumn concentrations are one order of magnitude lower. The  
 269 comparison between these sites reveals a different diurnal variation of HOMs. At SMEAR I, the HOMs have  
 270 a maximum around noon, spanning to the afternoon (Figure 3). At SMEAR II, HOMs have two maxima, one  
 271 at noon and another one in the early evening. From these, the latter is connected to non-nitrate monomer and  
 272 dimer HOMs and nitrate dimer HOMs. At SMEAR I the lack of an evening maximum could indicate that  
 273 HOM dimer formation is less dominant at SMEAR I compared to SMEAR II due to lower air temperatures,  
 274 or due to the different diurnal cycle of oxidants due to longer hours of solar radiation North of the Arctic Circle.

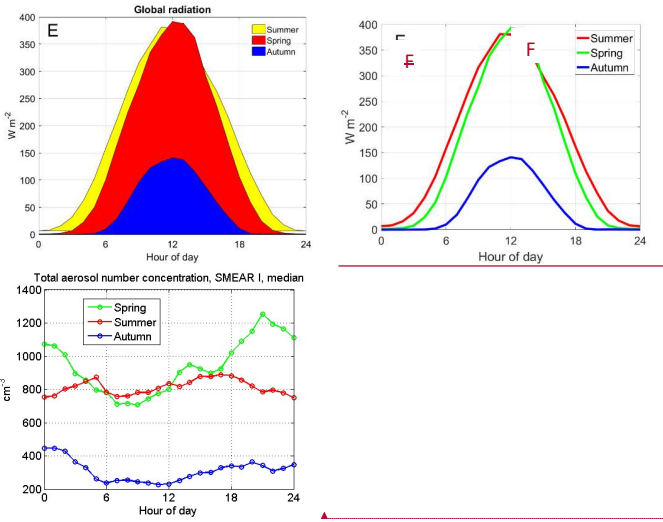
275



276

277

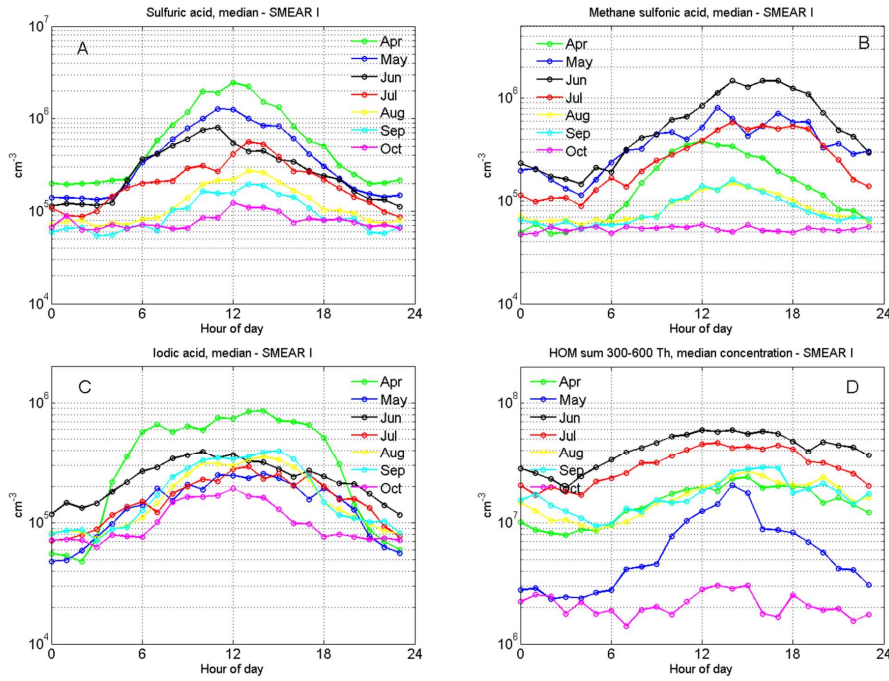
278



279 **Figure 3.** Diurnal variation of aerosol precursor gas median concentrations in different seasons: A) sulfuric  
280 acid, B) methane sulfonic acid, C) iodic acid and D) the sum of HOMs in the 300 to 600  $\text{Th}$  mass range. Panel  
281 E) depicts the seasonal variation of global radiation and F) the total aerosol number concentration  $N_{\text{tot}}$ . The  
282 small (false) offset ( $6\text{--}7 \text{ W m}^{-2}$ ) in summer data is due to 24 h sunlight hours at Värrö.

283 When analyzing the monthly aerosol precursor profiles in Figure 4, we observe that the springtime atmosphere  
284 is abundant in SA and iodic acidIA that have the highest median concentrations in April. MSA and HOMs  
285 concentrations peak in June. The MSA behavior is likely connected to the algae blooms in the Arctic Ocean  
286 that peak around midsummer. The marine emissions of DMS oxidize in the atmosphere to sulfur dioxide,  
287 sulfuric acidSA and to MSA (e.g. Park et al., 2018). However, sulfuric acidSA has more sources, since  $\text{SO}_2$ ,  
288 has also anthropogenic sources. At SMEAR I we cannot distinguish these sources precisely (more discussion  
289 about this in sectionSect 3.3.). It is notable that the peak concentration of MSA is earlier in the day in April,  
290 around 12 o'clock noon, than it is later in the year when the peak concentration is reached in the late afternoon  
291 (from 13:00 to 18:00 o'clock). There are no previous MSA concentration reports from the SMEAR stations  
292 but some gas phase MSA results from Antarctica show maximum of  $1 \cdot 10^5 \text{ cm}^{-3}$  to  $1 \cdot 10^7 \text{ cm}^{-3}$  concentrations  
293 (Jokinen et al., 2018; Mauldin et al., 2010, 2004). In the Arctic, around half a year measurement series from  
294 Villum in Greenland show MSA concentrations  $< 10^6 \text{ cm}^{-3}$  (Mar – Sep) and from  $10^5 \text{ cm}^{-3}$  to  $10^7 \text{ cm}^{-3}$  with the  
295 highest concentrations in June in Ny-Ålesund (Beck et al., 2021). Our measurements from the SMEAR I fall  
296 in between these extremes.

Formatted: English (United Kingdom)



297

298 **Figure 4.** Monthly median concentrations of A) sulfuric acid, B) methane sulfonic acid, C) iodic acid and d)  
 299 the sum of HOMs in the 300 to 600 Th mass range.

300 These are also the first reported results of *iodic-acidIA* measurements from SMEAR I and they represent a  
 301 continental location, the White Sea coast being ~130 km South East and the Barents *seaSea* ~230 km to the  
 302 North East. *iodic-acidIA*, iodine and iodic oxoacid emissions are commonly connected to coastal or marine  
 303 environments (Baccarini et al., 2020; McFiggans et al., 2010; O'dowd et al., 2002; Sipilä et al., 2016; Yu et  
 304 al., 2019) due to the fact that the ocean surface is a major source of iodine (Carpenter et al., 2013). While it is  
 305 not precisely known how *iodic-acidIA* forms in the gas phase, its formation requires oxidation of the initial  
 306 precursors (IO<sub>x</sub> species) by ozone and the last steps of its formation is potentially driven by reaction with OH  
 307 (Chameides and Davis, 1980).

308 Compared to the other precursor compounds, *iodic-acidIA* has the most stable concentration between seasons,  
 309 with a long increasing period in April during the snow-melting season. This is likely due to the simultaneously  
 310 increasing ozone mixing ratios (Figure 2D) and solar radiation. In contrast to measurements from the Arctic  
 311 Ocean (Baccarini et al., 2020), we did not observe a clear increase in *iodic-acidIA* concentration in the autumn  
 312 due to freezing. We find that September had only marginally higher concentrations compared to August or  
 313 July (Figure 4). Winter measurements would be necessary to estimate the effect of freezing in the concentration  
 314 of IA.

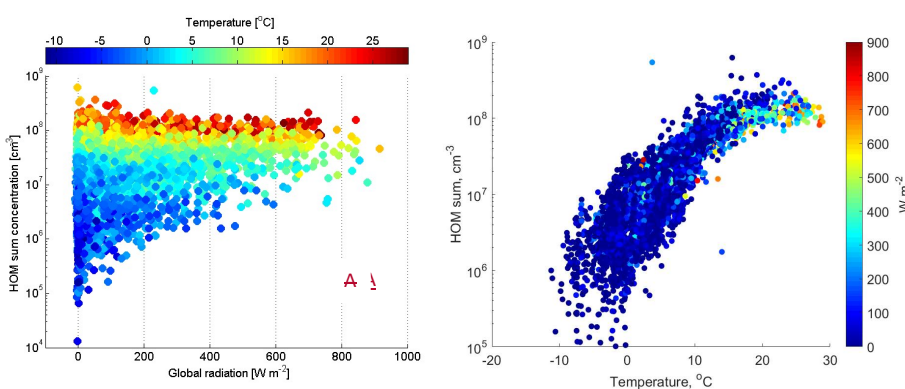
315 The source of *iodic-acidIA* on a continental site like the SMEAR I is an interesting subject to speculate. The  
 316 observed HIO<sub>3</sub> peak in April could indicate that there could be an influence from air masses exposed to Arctic  
 317 marine environment, *due to ocean surface acting as a major source of atmospheric iodine (Carpenter et al.,*  
 318 *2013)*. The increasing temperature in the spring induce a higher activity of phytoplankton in the nearby  
 319 Barents Sea and Norwegian Sea that remains ice free, even during the winter, and could result in the higher  
 320 emission of precursors for *iodic-acidIA* (Lai et al., 2011). Higher temperature would also result in more

321 efficient advection, which would transport species faster from emission points to SMEAR I. The calculated  
 322 back trajectories support the idea that iodine-rich air masses arrive from the West or northwest to SMEAR I  
 323 (discussed in details in [section 3.3. New Particle Formation events](#)[Sect 3.3](#), and Figure 10). This would be the  
 324 hypothesis of the long-range transport for source of [iodine-acidIA](#) in SMEAR I. On the contrary, the strong  
 325 diurnal variation on [iodine-acidIA](#) concentration seen as one order of magnitude difference between noon and  
 326 midnight, suggests fast on-site chemistry, which is not consistent with long-range transport of [iodine-acidIA](#),  
 327 but its precursor such as  $\text{CH}_3\text{I}$  (Bell et al., 2002). Also, [iodine-acidIA](#) life time against condensational loss is  
 328 expected to be short with the condensation sink at the site (Figure 2H), in the range of ~15 minutes, this  
 329 suggests that  $\text{HIO}_3$  is formed close to or at the site of measurements. Land vegetation is a source of methyl  
 330 iodide ( $\text{CH}_3\text{I}$ ) that could be the source of [iodine-acidIA](#) at SMEAR I, at least during summer (Sive et al., 2007).

331 Most interestingly, we seem to have an emission source of iodine during all seasons. There are no reports on  
 332 iodine emissions from continental snow, but we hypothesize that one possible source of iodine in SMEAR I  
 333 during spring is the snowpack. This is possible due to the deposition of sea salts on snow particularly during  
 334 dark periods that activate during the spring and are re-emitted to the atmosphere through heterogeneous  
 335 photochemistry of iodide, and iodate ions (Raso et al., 2017; Spolaor et al., 2019). There are also possible  
 336 forest emissions of iodinated organics, similar to New England growing season (Raso et al., 2017)<sup>7</sup> that might  
 337 be enhanced by higher temperature or high ozone concentrations. This type of emissions of iodinated gases,  
 338 or their implications, have not been studied before but these observations might direct research into emission  
 339 studies at SMEAR I, since our findings indicate that vegetation could be an emission source of iodine.

340 The sum of HOMs [in SMEAR I](#) reaches up to a median  $\sim 5 \cdot 10^7 \text{ cm}^{-3}$  concentration in the summer. This is  
 341 about one order of magnitude lower than the concentrations reported from the SMEAR II station in Hyttilä  
 342 (Yan et al., 2016) about 700 km south, where HOMs are at a maximum of  $\sim 6 \cdot 10^8 \text{ cm}^{-3}$  during spring daytime.  
 343 It is striking how well the concentration of HOMs follow the air temperature (Figure 5) but seem to level above  
 344 circa 18°C. From the temperature dependency, we can speculate that most VOCs emitted by vegetation close  
 345 to Väriö could be monoterpenes due to their strong temperature dependency. This is supported by emission  
 346 rate measurements of VOCs showing that in northern Finland 60 to 85 % are accounted by  $\alpha$ - and  $\beta$ -pinene  
 347 emissions (Tervainen et al., 2004). However, sesquiterpene emissions from nearby wetlands could contribute  
 348 to HOMs since their emissions are also temperature dependent and they are emitted by the boreal wetlands  
 349 (Hellén et al., 2020; Seco et al., 2020). As HOMs are oxidation products of VOCs, it is evident that the HOM  
 350 concentration will increase in SMEAR I in the future with the increasing VOC emissions, including isoprene,  
 351 monoterpenes and sesquiterpenes, due to temperature rise (Ghirardo et al., 2020; Tiiva et al., 2008; Valolahti  
 352 et al., 2015).

353



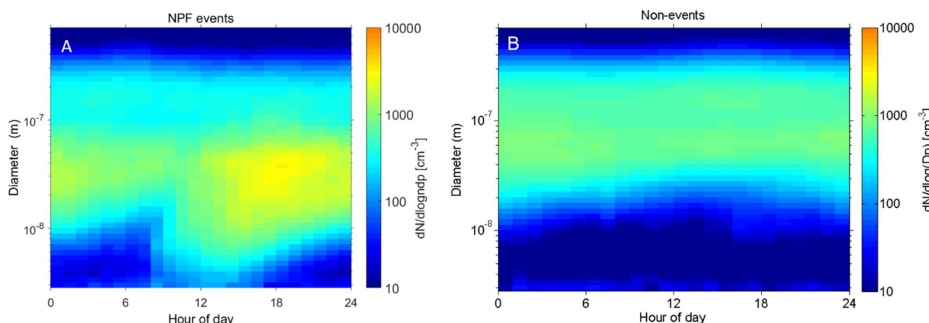
354 **Figure 5.** HOM concentration ( $\text{cm}^{-3}$ ) measured at SMEAR I (sum of mass range from 300 to 600 Th) as a  
 355 function of global radiation ( $\text{W m}^{-2}$ ) in panel A and as a function of temperature in panel B. The color bar  
 356 represents air temperature in  $^{\circ}\text{C}$  (A) and global radiation (B). The plot includes all data measured from April  
 357 to October 2019.

358 **3.3. New particle formation events:**

359 During the measurement period from 4 April 2019 to 27 October 2019, we observed 36 regional NPF events  
 360 in total and our CI-APi-TOF data covers 33 of these NPF days. During the same period, we observed 75 non-  
 361 event days without clear signs of particle formation (Maso et al., 2005). Rest of the days during our  
 362 measurement period were defined as undefined, bad data or partly bad data days and these were excluded from  
 363 our analysis. In this chapter, we focus on trace gases, meteorological parameters and detected aerosol precursor  
 364 gases during NPF days and compare them to non-event days.

365 We plot NPF and non-event days median average number size distribution of aerosol particles (from 3 to 800  
 366 nm) in Figure 6, and the total number concentration and the 2-7 nm air ion concentrations in Figure 7. The  
 367 whole measurement period is represented already in Figure 2. In figure 6, in the case of NPF event days we  
 368 see a distinct “banana” plot, where small  $< 10$  nm, particles are forming and growing with time. The DMPS  
 369 data is plotted from 2.82 nm to 708 nm but note that the channels below  $\sim 5$  nm have much larger uncertainties  
 370 than those above. The median event start time is located around noon and the growth of particles continues  
 371 steadily until midnight. However, when looking at individual days, there is a large variation in the start-times  
 372 of the particle formation, some events start early in the morning or even in the night, while some start in late  
 373 afternoon. Non-event days show very few particles in the  $< 10$  nm size bins.

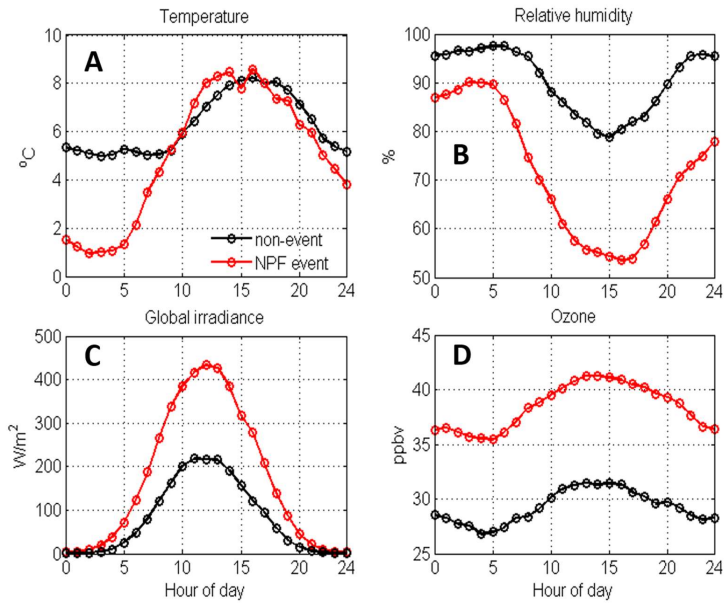
374 The total number of particles measured at the site during NPF events rises up to  $\sim 2400 \text{ cm}^{-3}$  reaching the  
 375 maximum concentration at  $\sim 17$  o'clock in the evening. This shows that NPF is an important source of aerosol  
 376 particles in Värrö as previously reported (Vehkamäki et al., 2004). Non-event days have clearly lower particle  
 377 concentrations throughout the day, staying lower than  $1000 \text{ cm}^{-3}$  on average. The measured 2-7 nm anion  
 378 concentrations stay very low during non-event days. As intermediate ions form mainly during NPF, their  
 379 concentrations are used as indicator of NPF events in boreal environments (Leino et al., 2016). On NPF days,  
 380 we see a peak in the anion concentration at noon, the concentration being about six times higher than during  
 381 non-event days. This indicates that negative ions may play a role in SMEAR I particle formation events.



382 **383 Figure 6.** This figure depicts the median number size distribution during all observed NPF events ( $n = 33$ ) and  
 384 non-events ( $n = 75$ ) during our measurement period. The data is collected with a DMPS and size bins from  
 385 2.82 to 708 nm are plotted.

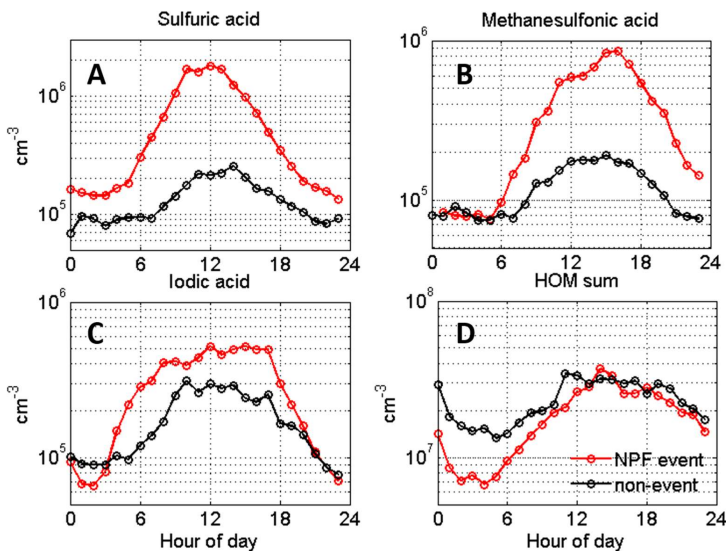
387 **Figure 7.** Median total particle concentration ( $N_{tot}$ ) in A) and 2-7 nm negative ion concentrations in B) at  
 388 SMEAR I during NPF event (red,  $n = 33$ ) and non-event days (black,  $n = 75$ ). The total particle number  
 389 concentration is recorded with a CPC and air ion concentrations with a NAIS.

390 Figure 8 shows the differences in temperature, [relative humidity](#), global radiation and ozone mixing ratios  
 391 between NPF event days (in red) and non-event days (black). In Värrö, NPF events preferably happen in  
 392 relatively low temperatures (1 – 8 °C) with a fast temperature rise in the early morning hours, lower and  
 393 decreasing RH, dropping from 90% to ~55 %, during the NPF days compared to non-event days. NPF days  
 394 have clearly higher global irradiance values (~450  $m^{-2}$  vs. ~200  $m^{-2}$ ) and about 10 ppbv higher ozone  
 395 concentrations than non-event days. The meteorological conditions favor NPF are thus similar than at the  
 396 SMEAR II station in Hyytiälä, where sunny clear sky days with low RH and condensation sink along with  
 397 wind directions from the cleaner northerly sector are forecasting NPF events (Niemi et al., 2014).



399 **Figure 8.** Average temperature (°C) in panel A), relative humidity (%) in B), global radiation (W m<sup>-2</sup>) in C)  
 400 and ozone concentration (ppbv) in D), all measured at SMEAR I during NPF event (red, n = 33) and non-event  
 401 days (black, n = 75).

402 Next, we show the concentrations of aerosol precursor compounds during NPF and non-event days in figure  
 403 9. The **sulfuric acid** (SA) concentrations closely follow the solar irradiation profile (Figure 8C). Similarly to the  
 404 results obtained from the high Arctic, Svalbard, also MSA is elevated during NPF events, especially during  
 405 summer, and could possibly contribute aerosol growth (Beck et al., 2021). We observe close to an order of  
 406 magnitude higher MSA concentration between the events and non-events days, highlighting the dominant role  
 407 of sulfur species to nucleation and growth in general at this site. In order to attribute the source of sulfur species  
 408 and IA during the event and non-event days we performed a cluster analysis using a geographical information  
 409 system (GIS) based software, Trajstat (Wang et al., 2009). The NCEP/NCAR reanalysis data was used as  
 410 meteorological input for the model (Kalnay et al., 1996). The simulations were performed at an arrival height  
 411 of 250 m. a.g.l. SMEAR I station is located approximately at similar height (390 m a.s.l.), thus representing the  
 412 air masses arriving at the station even during strong temperature inversions (Sipilä et al., 2021).

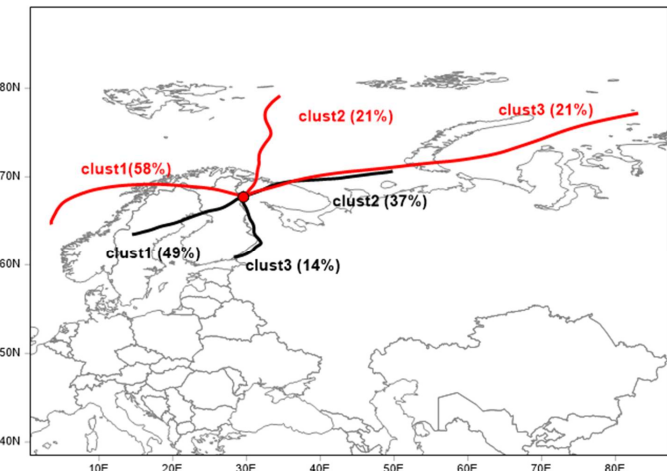


413  
 414 **Figure 9.** Aerosol precursor gases in SMEAR I during NPF (red, n = 33) and non-event days (black, n = 75).  
 415 The data is hourly median average.

416 Higher concentrations of aerosol precursors SA, MSA and IA are connected to the air masses that arrive to  
 417 SMEAR I from the Arctic Ocean (Figure 10). Cluster analysis of air mass back trajectories arriving to Väriö  
 418 during NPF days clearly shows, that most NPF events occur when the air mass was exposed to marine  
 419 environments within the last 72 hours. In our case, mainly the Norwegian Sea in the West (58 %) or the Barents  
 420 (21 %) and Kara Seas (21 %) in the Arctic Ocean. This seems relevant to our results since the marine  
 421 environment in the North is emitting large amounts of **dimethyl sulfide** (DMS), a precursor for SA and MSA  
 422 (Levasseur, 2013) and iodine species that further oxidize to IA (Baccarini et al., 2020; Sherwen et al., 2016).  
 423 A fraction of air masses that are connected to both NPF (21 %) and non-event days (37 %) are coming to  
 424 SMEAR I from the Kola peninsula that is connected to high SO<sub>2</sub> emissions, higher particle number  
 425 concentrations and winter time NPF events (Sipilä et al., 2021). Most non-event air masses arrive to Väriö  
 426 from South-West (49 %) crossing northern Finland and Sweden.

427 In addition from Figure 9 we observe that we cannot rule out the contribution of iodine-acidIA in NPF in  
 428 SMEAR I, but with the recorded concentration, it usually is not enough to initiate NPF (He et al., 2021).  
 429 Although iodine-acidIA concentrations are slightly larger on NPF days than non-event days, the rise in  
 430 concentration happens already early in the morning, clearly before the average event start-time. The possible  
 431 source of iodine-acidIA was discussed earlier in chapterSect 3.2 and we hypothesize that the source of iodine at  
 432 SMEAR I could be both; i) the long distance transport from the Arctic Ocean combined to ii) the local  
 433 emissions from the snow pack and vegetation. The hypothesis of vegetation emitted iodine species is supported  
 434 by the minor difference between NPF (mostly marine) and non-event day (mostly continental) concentrations.  
 435 At SMEAR I, HOMs are the only species that are at a (marginally) lower level during non-event than NPF  
 436 days indicating that the total HOM concentration does not determine when NPF events occur. However, this  
 437 does not exclude the possible participation of certain HOMs in NPF together with sulfur compounds (Lehtipalo  
 438 et al., 2018) or at later stages of the NPF process, especially during particle growth. However, pure biogenic  
 439 nucleation involving ions and HOMs (Kirkby et al., 2016) seems not to be a major NPF pathway in Värrö.

440 Our measurements do not unveil the detailed mechanism of nucleation or growth of particles. We lack  
 441 measurements of ambient bases that are needed to stabilize sulfuric acidSA clusters in ambient conditions (e.g.  
 442 Almeida et al., 2013; Jen et al., 2014; Kirkby et al., 2011; Kürten et al., 2014; Myllys et al., 2018). With the  
 443 given observations comparing NPF days with non-event days it is likely that most regional NPF events require  
 444 sulfuric acidSA, but the NPF process can involve other compounds as well, especially IA and MSA, which  
 445 show higher concentrations on NPF days, very similarly that the results reported from Ny-Ålesund (Beck et  
 446 al., 2021).



447  
 448 **Figure 10.** Trajectory cluster analysis of 72-hour back trajectories simulated at arrival height of 250 m a.g.l  
 449 and the NCEP/NCAR reanalysis data used as meteorological input. Red = NPF event, black = non-NPF

450 **4. Conclusions:**

451 We report ~7 months of nitrate-based CI-APi-TOF measurements of sulfuric acid, methane sulfonic acid, iodine  
 452 acidSA, MSA, IA and highly oxygenated organic compoundsHOM from a remote sub-Arctic field station  
 453 SMEAR I in Finland. The measurements aim to increase our understanding of the Arctic aerosol forming  
 454 precursors and atmospheric chemistry in more details. The reason for measuring these compounds ~150 km  
 455 north of the Arctic Circle is simple; the Arctic is warming twice the speed as the planet on average. Lapland is  
 456 already facing environmental changes when e.g. woody plants disperse further north and influence the tundra

457 ecosystem (Aakala et al., 2014; Kemppinen et al., 2021). These changes will in turn affect the emissions of  
458 aerosol precursor gases, which may have feedback effects on to the climate (e.g. Kulmala et al., 2020; Paasonen  
459 et al., 2013).

460 The area surrounding SMEAR I station has snow cover for almost 8 months a year. Accumulating snow during  
461 the autumn is a good reservoir to e.g. halogens, similarly than in the high Arctic (and Arctic Ocean)  
462 environment. The snow pack also acts as a cover for biogenic emissions entering the atmosphere from the  
463 ground. Any changes in the temperature and snow cover in the sub-Arctic regions will effect on atmospheric  
464 chemistry and composition that are undeniably changing the way aerosol particles form and what their number  
465 concentration is in the region.

466 In this study, we report seasonal and monthly variations of SA, MSA, IA and HOM concentrations and find  
467 all these compounds abundant in springtime. SA has a peak concentration in the spring, decreasing for the rest  
468 of the seasons. We detect high concentrations of MSA and IA that are usually connected to marine and coastal  
469 environments, although Värrjö is located ~130 km from the nearest coast of the White Sea. While MSA is  
470 abundant in the spring, summer and decreases to limit of detection levels for autumn, IA continues at the same  
471 concentration throughout the seasons. It seems likely that these two compounds are connected to emissions  
472 from phytoplankton or the Arctic ice pack and arrive to SMEAR I by long transport routes. In the case of ~~iodine~~  
473 ~~acid~~IA, we suggest that the source of iodine emissions is a combination of transport and local emission from  
474 the continental snow pack and vegetation at the site. Further work is needed to confirm this hypothesis.

475 The most striking correlation we found in HOM concentrations and ambient air temperature. The vegetation  
476 at SMEAR I is the source of VOCs even in the snow covered spring season and these volatile gases are oxidized  
477 into HOMs with different reaction rates depending on the oxidant. In the case of such strong temperature  
478 controlled HOM concentrations, we conclude that HOMs in the mass range of 300 – 600 Th are most likely  
479 products of monoterpene oxidation.

480 We also studied the abundance of these aerosol precursors separately during NPF and non-event days. We  
481 observed that new particles at SMEAR I preferably form in relatively low temperatures (< 10°C), low ~~relative~~  
482 ~~humidity~~RH that decreases with rising temperature during the day (to a minimum of ~55%), ~10 ppbv higher  
483 ozone mixing ratio than during non-event days, high SA concentration in the morning and high MSA  
484 concentrations in the afternoon. Cluster analysis of air masses show that NPF usually happens in marine air  
485 masses travelling to the site from North West – West. All together, these are the first long term measurements  
486 of aerosol forming precursor from the sub-arctic region helping us to understand atmospheric chemical  
487 processes and aerosol formation in the rapidly changing Arctic.

#### 488 **Data availability:**

489 All meteorological parameters, trace gas concentrations and aerosol data we downloaded directly from  
490 smartSMEAR open access database (<https://smear.avaa.csc.fi/>). ~~All mass~~Mass spectrometric data, ~~event~~  
491 ~~analysis, condensation sink and anion concentration data~~ are available on ~~request from the corresponding~~  
492 ~~author~~Zenodo, <https://doi.org/10.5281/zenodo.5879549>.

#### 493 **Author contribution:**

494 TJ, MS, TP and MK designed the experiments at SMEAR I and MS, NS, KN and TL carried them out. IY  
495 made the NPF event analysis and RT calculated the back trajectories. TJ and KL wrote the manuscript with  
496 contributions from all co-authors.

#### 497 **Competing interests:**

498 Markku Kulmala is editor of ACP. Tuukka Petäjä is editor of ACP.

#### 499 **Acknowledgements:**

500 We would like to thank the technical staff in Kumpula and Väriö, who keep the long-term measurements  
501 going and helped with data collection, instrument calibrations, logistics and in data quality control and  
502 assurance during the year. We acknowledge the important role our collaborators have in scientific discussion  
503 and a special thanks goes to Alfonso Saiz-Lopez for [iodine-acidIA](#) related discussion that helped to draft this  
504 article. We thank the ACTRIS CiGas-UHEL unit for mass spectrometer calibration support and the tofTools  
505 team for data analysis software.

506 **Financial support:**

507 The Academy of Finland via Center of Excellence in Atmospheric Sciences (project no. 272041) and European  
508 Research Council via ATM-GTP 266 (742206), GASPARCON (714621) and Flagship funding (grant no.  
509 337549) funded this work. We also received funding from the Academy of Finland (project no. 1235656,  
510 296628, 316114, 315203, 307537, 325647, 33397, 334792 and 334514) “Quantifying carbon sink,  
511 CarbonSink+ and their interaction with air quality” and Academy professorship (grant no. 302958). This work  
512 was further supported by the European Commission via via project iCUPE (Integrative and Comprehensive  
513 Understanding on Polar Environments, No 689443), the EMME-CARE project which received funding from  
514 the European Union's Horizon 2020 Research and Innovation Programme, under grant agreement no. 856612,  
515 Regional Council of Lapland (Väriön tutkimusaseman huippututkimus hyödyntämään Itä-Lapin  
516 elinkeinoelämää, VÄRI, A74190) and Aatos Erkko Foundation.

517 **References:**

518 Aakala, T., Hari, P., Dengel, S., Newberry, S. L., Mizunuma, T. and Grace, J.: A prominent stepwise  
519 advance of the tree line in north-east Finland, *J. Ecol.*, 102(6), 1582–1591, doi:10.1111/1365-2745.12308,  
520 2014.

521 Ahonen, T., Aalto, P., Rannik, Ü., Kulmala, M., Nilsson, E. D., Palmroth, S., Ylitalo, H. and Hari, P.:  
522 Variations and vertical profiles of trace gas and aerosol concentrations and CO<sub>2</sub> exchange in eastern  
523 Lapland, *Atmos. Environ.*, 31(20), 3351–3362, doi:10.1016/S1352-2310(97)00151-9, 1997.

524 Almeida, J., Schobesberger, S., Kürten, A., Ortega, I. K., Kupiainen-Määttä, O., Praplan, A. P., Adamov, A.,  
525 Amorim, A., Bianchi, F., Breitenlechner, M., David, A., Dommen, J., Donahue, N. M., Downard, A., Dunne,  
526 E., Duplissy, J., Ehrhart, S., Flagan, R. C., Franchin, A., Guida, R., Hakala, J., Hansel, A., Heinritzi, M.,  
527 Henschel, H., Jokinen, T., Junninen, H., Kajos, M., Kangasluoma, J., Keskinen, H., Kupc, A., Kurtén, T.,  
528 Kvashin, A. N., Laaksonen, A., Lehtipalo, K., Leiminger, M., Leppä, J., Loukonen, V., Makhmutov, V.,  
529 Mathot, S., McGrath, M. J., Nieminen, T., Olenius, T., Onnela, A., Petäjä, T., Riccobono, F., Riipinen, I.,  
530 Rissanen, M., Rondo, L., Ruuskanen, T., Santos, F. D., Sarnela, N., Schallhart, S., Schnitzhofer, R., Seinfeld,  
531 J. H., Simon, M., Sipilä, M., Stozhkov, Y., Stratmann, F., Tomé, A., Tröstl, J., Tsagkogeorgas, G.,  
532 Vaattovaara, P., Viisanen, Y., Virtanen, A., Vrtala, A., Wagner, P. E., Weingartner, E., Wex, H.,  
533 Williamson, C., Wimmer, D., Ye, P., Yli-Juuti, T., Carslaw, K. S., Kulmala, M., Curtius, J., Baltensperger,  
534 U., Worsnop, D. R., Vehkämäki, H. and Kirkby, J.: Molecular understanding of sulphuric acid-amine  
535 particle nucleation in the atmosphere, *Nature*, 502(7471), 359–363, doi:10.1038/nature12663, 2013.

536 Baccarini, A., Karlsson, L., Dommen, J., Duplessis, P., Vüllers, J., Brooks, I. M., Saiz-Lopez, A., Salter, M.,  
537 Tjernström, M., Baltensperger, U., Zieger, P. and Schmale, J.: Frequent new particle formation over the high  
538 Arctic pack ice by enhanced iodine emissions, *Nat. Commun.*, 11(1), doi:10.1038/s41467-020-18551-0,  
539 2020.

540 Beck, L. J., Sarnela, N., Junninen, H., Hoppe, C. J. M. M., Garmash, O., Bianchi, F., Riva, M., Rose, C.,  
541 Peräkylä, O., Wimmer, D., Kausiala, O., Jokinen, T., Ahonen, L., Mikkilä, J., Hakala, J. J., He, X.-C. C.,  
542 Kontkanen, J., Wolf, K. K. E. E., Cappelletti, D., Mazzola, M., Traversi, R., Petroselli, C., Viola, A. P.,  
543 Vitale, V., Lange, R., Massling, A., Nøjgaard, J. K., Krejci, R., Karlsson, L., Zieger, P., Jang, S. S., Lee, K.,  
544 Vakkari, V., Lampilahti, J., Thakur, R. C., Leino, K., Kangasluoma, J., Duplissy, E.-M. M., Siivola, E.,  
545 Marbouti, M., Tham, Y. J., Saiz-Lopez, A., Petäjä, T., Ehn, M., Worsnop, D. R., Skov, H., Kulmala, M.,  
546 Kerminen, V.-M. M., Sipilä, M., Nøjgaard, J., Krejci, R., Karlsson, L., Zieger, P., Jang, S. S., Lee, K.,  
547 Vakkari, V., Lampilahti, J., Thakur, R. C., Leino, K., Kangasluoma, J., Duplissy, E.-M. M., Siivola, E.,

548 Marbouti, M., Tham, Y. J., Saiz-Lopez, A., Petäjä, T., Ehn, M., Worsnop, D. R., Skov, H., Kulmala, M.,  
 549 Kermoisen, V.-M. M. and Sipilä, M.: Differing Mechanisms of New Particle Formation at Two Arctic Sites,  
 550 *Geophys. Res. Lett.*, 48(4), e2020GL091334, doi:10.1029/2020GL091334, 2021.

551 Bell, N., Hsu, L., Jacob, D. J., Schultz, M. G., Blake, D. R., Butler, J. H., King, D. B., Lobert, J. M. and  
 552 Maier-Reimer, E.: Methyl iodide: Atmospheric budget and use as a tracer of marine convection in global  
 553 models, *J. Geophys. Res. Atmos.*, 107(D17), ACH 8-1, doi:10.1029/2001JD001151, 2002.

554 Berndt, T., Richters, S., Jokinen, T., Hyttinen, N., Kurtén, T., Otkjær, R. V., Kjaergaard, H. G., Stratmann,  
 555 F., Herrmann, H., Sipilä, M., Kulmala, M. and Ehn, M.: Hydroxyl radical-induced formation of highly  
 556 oxidized organic compounds, *Nat. Commun.*, 7, 13677, doi:10.1038/ncomms13677, 2016.

557 Bianchi, F., Garmash, O., He, X., Yan, C., Iyer, S., Rosendahl, I., Xu, Z., Rissanen, M. P., Riva, M., Taipale,  
 558 R., Sarnela, N., Petäjä, T., Worsnop, D. R., Kulmala, M., Ehn, M. and Junninen, H.: The role of highly  
 559 oxygenated molecules (HOMs) in determining the composition of ambient ions in the boreal forest, *Atmos.  
 560 Chem. Phys.*, 17(22), 13819–13831, doi:10.5194/acp-17-13819-2017, 2017.

561 Bradshaw, C. J. A. and Warkentin, I. G.: Global estimates of boreal forest carbon stocks and flux, *Glob.  
 562 Planet. Change*, 128, 24–30, doi:10.1016/j.gloplacha.2015.02.004, 2015.

563 Brandt, J. P., Flannigan, M. D., Maynard, D. G., Thompson, I. D. and Volney, W. J. A.: An introduction to  
 564 Canada's boreal zone: Ecosystem processes, health, sustainability, and environmental issues1, *Environ. Rev.*,  
 565 21(4), 207–226, doi:10.1139/er-2013-0040, 2013.

566 Carpenter, L. J., MacDonald, S. M., Shaw, M. D., Kumar, R., Saunders, R. W., Parthipan, R., Wilson, J. and  
 567 Plane, J. M. C.: Atmospheric iodine levels influenced by sea surface emissions of inorganic iodine, *Nat.  
 568 Geosci.*, 6(2), 108–111, doi:10.1038/ngeo1687, 2013.

569 Chameides, W. L. and Davis, D. D.: Iodine: Its possible role in tropospheric photochemistry, *J. Geophys.  
 570 Res. Ocean.*, 85(C12), 7383–7398, doi:10.1029/JC085IC12P07383, 1980.

571 Charlson, R. J., Lovelock, J. E., Andreae, M. O. and Warren, S. G.: Oceanic phytoplankton, atmospheric  
 572 sulphur, cloud albedo and climate, *Nature*, 326(6114), 655–661, doi:10.1038/326655a0, 1987.

573 Dal Maso, M., Sogacheva, L., Aalto, P. P., Riipinen, I., Komppula, M., Tunved, P., Korhonen, L., Suur-Uski,  
 574 V., Hirsikko, A., Kurtén, T., Kermoisen, V.-M. M., Lihavainen, H., Viisanen, Y. Y., Hansson, H.-C. C.,  
 575 Kulmala, M., Maso, M. D., Sogacheva, L., Aalto, P. P., Riipinen, I., Komppula, M., Tunved, P., Korhonen,  
 576 L., Suur-Uski, V., Hirsikko, A., Kurtén, T., Kermoisen, V.-M. M., Lihavainen, H., Viisanen, Y. Y., Hansson,  
 577 H.-C. C., Kulmala, M., Dal Maso, M., Sogacheva, L., Aalto, P. P., Riipinen, I., Komppula, M., Tunved, P.,  
 578 Korhonen, L., Suur-Uski, V., Hirsikko, A., Kurtén, T., Kermoisen, V.-M. M., Lihavainen, H., Viisanen, Y.  
 579 Y., Hansson, H.-C. C., Kulmala, M.: Aerosol size distribution measurements at four Nordic field stations:  
 580 Identification, analysis and trajectory analysis of new particle formation bursts, *Tellus, Ser. B Chem. Phys.  
 581 Meteorol.*, 59(3), 350–361, doi:10.1111/j.1600-0889.2007.00267.x, 2007.

582 Dall Osto, M., Geels, C., Beddows, D. C. S., Boertmann, D., Lange, R., Nøjgaard, J. K., Harrison, R. M.,  
 583 Simo, R., Skov, H. and Massling, A.: Regions of open water and melting sea ice drive new particle formation  
 584 in North East Greenland., *Sci. Rep.*, 8(1), 6109, doi:10.1038/s41598-018-24426-8, 2018.

585 Ehn, M., Thornton, J. A., Kleist, E., Sipilä, M., Junninen, H., Pullinen, I., Springer, M., Rubach, F.,  
 586 Tillmann, R., Lee, B., Lopez-Hilfiker, F., Andres, S., Acir, I.-H. H., Rissanen, M., Jokinen, T.,  
 587 Schobesberger, S., Kangasluoma, J., Kontkanen, J., Nieminen, T., Kurtén, T., Nielsen, L. B., Jørgensen, S.,  
 588 Kjaergaard, H. G., Canagaratna, M., Maso, M. D., Berndt, T., Petäjä, T., Wahner, A., Kermoisen, V.-M. M.,  
 589 Kulmala, M., Worsnop, D. R., Wildt, J. and Mentel, T. F.: A large source of low-volatility secondary organic  
 590 aerosol, *Nature*, 506(7489), 476–479, doi:10.1038/nature13032, 2014.

591 Ghirardo, A., Lindstein, F., Koch, K., Buegger, F., Schloter, M., Albert, A., Michelsen, A., Winkler, J. B.,  
 592 Schnitzler, J.-P. and Rinnan, R.: Origin of volatile organic compound emissions from subarctic tundra under  
 593 global warming, *Glob. Chang. Biol.*, 26(3), 1908–1925, doi:10.1111/GCB.14935, 2020.

594 Hari, P., Aalto, P., Hämeri, K., Kulmala, M., Lahti, T., Luoma, S., Palva, L., Pohja, T., Pulliainen, E.,

595 Siivola, E. and Vesala, T.: Air pollution in eastern Lapland: challenge for an environmental measurement  
596 station, *Silva Fenn.*, 28(1), 29–39, doi:10.14214/SF.A9160, 1994.

597 He, X.-C., Tham, Y. J., Dada, L., Wang, M., Finkenzeller, H., Stolzenburg, D., Iyer, S., Simon, M., Kürten,  
598 A., Shen, J., Rörup, B., Rissanen, M., Schobesberger, S., Baalbaki, R., Wang, D. S., Koenig, T. K., Jokinen,  
599 T., Sarnela, N., Beck, L. J., Almeida, J., Amanatidis, S., Amorim, A., Ataei, F., Baccarini, A., Bertozi, B.,  
600 Bianchi, F., Brilke, S., Caudillo, L., Chen, D., Chiu, R., Chu, B., Dias, A., Ding, A., Dommen, J., Duplissy,  
601 J., Haddad, I. El, Carracedo, L. G., Granzin, M., Hansel, A., Heinritzi, M., Hofbauer, V., Junninen, H.,  
602 Kangasluoma, J., Kemppainen, D., Kim, C., Kong, W., Krechmer, J. E., Kvashin, A., Laitinen, T.,  
603 Lamkaddam, H., Lee, C. P., Lehtipalo, K., Leiminger, M., Li, Z., Makhmutov, V., Manninen, H. E., Marie,  
604 G., Marten, R., Mathot, S., Mauldin, R. L., Mentler, B., Möhler, O., Müller, T., Nie, W., Onnela, A., Petäjä,  
605 T., Pfeifer, J., Philippov, M., Ranjithkumar, A., Saiz-Lopez, A., Salma, I., Scholz, W., Schuchmann, S.,  
606 Schulze, B., Steiner, G., Stozhkov, Y., Tauber, C., Tomé, A., Thakur, R. C., Väistönen, O., Vazquez-Pufleau,  
607 M., Wagner, A. C., Wang, Y., Weber, S. K., Winkler, P. M., Wu, Y., Xiao, M., Yan, C., Ye, Q., Ylisirniö,  
608 A., Zauner-Wieczorek, M., Zha, Q., Zhou, P., Flagan, R. C., Curtius, J., Baltensperger, U., Kulmala, M.,  
609 Kermiinen, V.-M., Kurtén, T., et al.: Role of iodine oxoacids in atmospheric aerosol nucleation, *Science* (80-  
610 ), 371(6529), 589–595, doi:10.1126/SCIENCE.ABE0298, 2021.

611 Hellén, H., Schallhart, S., Praplan, A., Tykkä, T., Aurela, M., Lohila, A. and Hakola, H.: Terpenoid  
612 measurements at a Northern wetland revealed a strong source of sesquiterpenes, *Atmos. Chem. Phys.*  
613 Discuss., 1–20, doi:10.5194/ACP-2019-1154, 2020.

614 Hyttinen, N., Kupiainen-Määttä, O., Rissanen, M. P., Muuronen, M., Ehn, M. and Kurtén, T.: Modeling the  
615 Charging of Highly Oxidized Cyclohexene Ozonolysis Products Using Nitrate-Based Chemical Ionization, *J.*  
616 *Phys. Chem. A*, 119(24), 6339–6345, 2015.

617 IPCC, F. assessment report: Fifth Assessment Report - Climate Change 2013, IPCC, Fifth Assess. Rep. -  
618 Clim. Chang. [online] Available from: <http://www.ipcc.ch/report/ar5/wg1/>, 2013.

619 Jen, C. N., McMurry, P. H. and Hanson, D. R.: Stabilization of sulfuric acid dimers by ammonia,  
620 methylamine, dimethylamine, and trimethylamine, *J. Geophys. Res. Atmos.*, 119(12), 7502–7514,  
621 doi:10.1002/2014JD021592, 2014.

622 Jokinen, T., Sipilä, M., Junninen, H., Ehn, M., Lönn, G., Hakala, J., Petäjä, T., Mauldin, R. L., Kulmala, M.  
623 and Worsnop, D. R.: Atmospheric sulphuric acid and neutral cluster measurements using CI-APi-TOF,  
624 *Atmos. Chem. Phys.*, 12(9), 4117–4125, doi:10.5194/acp-12-4117-2012, 2012.

625 Jokinen, T., Sipilä, M., Richters, S., Kermiinen, V.-M. M., Paasonen, P., Stratmann, F., Worsnop, D.,  
626 Kulmala, M., Ehn, M., Herrmann, H. and Berndt, T.: Rapid autoxidation forms highly oxidized RO<sub>2</sub> radicals  
627 in the atmosphere, *Angew. Chemie Int. Ed.*, 53(52), 14596–14600, doi:10.1002/anie.201408566, 2014.

628 Jokinen, T., Kontkanen, J., Lehtipalo, K., Manninen, H. E., Aalto, J., Porcar-Castell, A., Garmash, O.,  
629 Nieminen, T., Ehn, M., Kangasluoma, J., Junninen, H., Levula, J., Duplissy, J., Ahonen, L. R., Rantala, P.,  
630 Heikkilä, L., Yan, C., Sipilä, M., Worsnop, D. R., Bäck, J., Petäjä, T., Kermiinen, V.-M. and Kulmala, M.:  
631 Solar eclipse demonstrating the importance of photochemistry in new particle formation., *Sci. Rep.*, 7,  
632 45707, doi:10.1038/srep45707, 2017.

633 Jokinen, T., Sipilä, M., Kontkanen, J., Vakkari, V., Tisler, P., Duplissy, E. M., Junninen, H., Kangasluoma,  
634 J., Manninen, H. E., Petäjä, T., Kulmala, M., Worsnop, D. R., Kirkby, J., Virkkula, A. and Kermiinen, V. M.:  
635 Ion-induced sulfuric acid–ammonia nucleation drives particle formation in coastal Antarctica, , 4(11),  
636 eaat9744, doi:10.1126/SCIAADV.AAT9744, 2018.

637 Junninen, H., Ehn, M., Petäjä, T., Luosujärvi, L., Kotiaho, T., Kostianen, R., Rohner, U., Gonin, M., Fuhrer,  
638 K., Kulmala, M. and Worsnop, D. R.: A high-resolution mass spectrometer to measure atmospheric ion  
639 composition, *Atmos. Meas. Tech.*, 3(4), 1039–1053, doi:10.5194/amt-3-1039-2010, 2010.

640 Kalnay, E., Kanamitsu, M., Kistler, R., Collins, W., Deaven, D., Gandin, L. and E. Kalnay M. Kanamitsu R.  
641 Kistler W. Collins D. Deaven L. Gandin M. Iredell S. Saha G. White J. Woollen Y. Zhu M. Chelliah W.  
642 Ebisuzaki W. HE. Kalnay M. Kanamitsu R. Kistler W. Collins D. Deaven L. Gandin M. Iredell S. Saha G.

643 White, and D. J.: The NCEP/NCAR 40-Year Reanalysis Project, *Bull. Am. Meteorol. Soc.*, 437–472,  
 644 doi:[https://doi.org/10.1175/1520-0477\(1996\)077<0437:TNYRP>2.0.CO;2](https://doi.org/10.1175/1520-0477(1996)077<0437:TNYRP>2.0.CO;2), 1996.

645 Kemppinen, J., Niittynen, P., Virkkala, A.-M., Happonen, K., Riihimäki, H., Aalto, J. and Luoto, M.: Dwarf  
 646 Shrubs Impact Tundra Soils: Drier, Colder, and Less Organic Carbon, *Ecosyst.* 2021, 1–15,  
 647 doi:10.1007/S10021-020-00589-2, 2021.

648 Kerminen, V.-M., Paramonov, M., Anttila, T., Riipinen, I., Fountoukis, C., Korhonen, H., Asmi, E., Laakso,  
 649 L., Lihavainen, H., Swietlicki, E., Svenningsson, B., Asmi, A., Pandis, S. N., Kulmala, M. and Petäjä, T.:  
 650 Cloud condensation nuclei production associated with atmospheric nucleation: a synthesis based on existing  
 651 literature and new results, *Atmos. Chem. Phys.*, 12(24), 12037–12059, doi:10.5194/acp-12-12037-2012,  
 652 2012.

653 Kerminen, V., Aurela, M., Hillamo, R. E. and Virkkula, A.: Formation of particulate MSA: deductions from  
 654 size distribution measurements in the Finnish Arctic, *Tellus B*, 49(2), 159–171, doi:10.1034/j.1600-  
 655 0889.49.issue2.4.x, 1997.

656 Kirkby, J., Curtius, J., Almeida, J., Dunne, E., Duplissy, J., Ehrhart, S., Franchin, A., Gagné, S., Ickes, L.,  
 657 Kürten, A., Kupc, A., Metzger, A., Riccobono, F., Rondo, L., Schobesberger, S., Tsagkogeorgas, G.,  
 658 Wimmer, D., Amorim, A., Bianchi, F., Breitenlechner, M., David, A., Dommen, J., Downard, A., Ehn, M.,  
 659 Flagan, R. C., Haider, S., Hansel, A., Hauser, D., Jud, W., Junninen, H., Kreissl, F., Kvashin, A., Laaksonen,  
 660 A., Lehtipalo, K., Lima, J., Lovejoy, E. R., Makhmutov, V., Mathot, S., Mikkilä, J., Minginette, P., Mogo,  
 661 S., Nieminen, T., Onnela, A., Pereira, P., Petäjä, T., Schnitzhofer, R., Seinfeld, J. H., Sipilä, M., Stozhkov,  
 662 Y., Stratmann, F., Tomé, A., Vanhanen, J., Viisanen, Y., Vrtala, A., Wagner, P. E., Walther, H.,  
 663 Weingartner, E., Wex, H., Winkler, P. M., Carslaw, K. S., Worsnop, D. R., Baltensperger, U. and Kulmala,  
 664 M.: Role of sulphuric acid, ammonia and galactic cosmic rays in atmospheric aerosol nucleation., *Nature*,  
 665 476(7361), 429–433, doi:10.1038/nature10343, 2011.

666 Kirkby, J., Duplissy, J., Sengupta, K., Frege, C., Gordon, H., Williamson, C., Heinritzi, M., Simon, M., Yan,  
 667 C., Almeida, J. J., Trostl, J., Nieminen, T., Ortega, I. K., Wagner, R., Adamov, A., Amorim, A.,  
 668 Bernhammer, A.-K. K., Bianchi, F., Breitenlechner, M., Brilke, S., Chen, X., Craven, J., Dias, A., Ehrhart,  
 669 S., Flagan, R. C., Franchin, A., Fuchs, C., Guida, R., Hakala, J., Hoyle, C. R., Jokinen, T., Junninen, H.,  
 670 Kangasluoma, J., Kim, J., Krapf, M., Kurten, A., Laaksonen, A., Lehtipalo, K., Makhmutov, V., Mathot, S.,  
 671 Molteni, U., Onnela, A., Perakyla, O., Piel, F., Petaja, T., Praplan, A. P., Pringle, K., Rap, A., Richards, N.  
 672 A. D. D., Riipinen, I., Rissanen, M. P., Rondo, L., Sarnela, N., Schobesberger, S., Scott, C. E., Seinfeld, J.  
 673 H., Sipila, M., Steiner, G., Stozhkov, Y., Stratmann, F., Tomé, A., Virtanen, A., Vogel, A. L., Wagner, A. C.,  
 674 Wagner, P. E., Weingartner, E., Wimmer, D., Winkler, P. M., Ye, P., Zhang, X., Hansel, A., Dommen, J.,  
 675 Donahue, N. M., Worsnop, D. R., Baltensperger, U., Kulmala, M., Carslaw, K. S., Curtius, J., Tröstl, J.,  
 676 Nieminen, T., Ortega, I. K., Wagner, R., Adamov, A., Amorim, A., Bernhammer, A.-K. K., Bianchi, F.,  
 677 Breitenlechner, M., Brilke, S., Chen, X., Craven, J., Dias, A., Ehrhart, S., Flagan, R. C., Franchin, A., Fuchs,  
 678 C., Guida, R., Hakala, J., Hoyle, C. R., Jokinen, T., et al.: Ion-induced nucleation of pure biogenic particles,  
 679 *Nature*, 533(7604), 521–526, doi:10.1038/nature17953, 2016.

680 Kulmala, M., Toivonen, A., Mäkelä, J. M. and Laaksonen, A.: Analysis of the growth of nucleation mode  
 681 particles observed in Boreal forest, *Tellus B*, 50(5), 449–462, doi:10.1034/j.1600-0889.1998.t01-4-00004.x,  
 682 1998.

683 Kulmala, M., Riipinen, I., Sipilä, M., Manninen, H. E., Petäjä, T., Junninen, H., Dal Maso, M., Mordas, G.,  
 684 Mirme, A., Vana, M., Hirsisiko, A., Laakso, L., Harrison, R. M., Hanson, I., Leung, C., Lehtinen, K. E. J. and  
 685 Kerminen, V. M.: Toward direct measurement of atmospheric nucleation, *Science* (80-.), 318(5847), 89–92,  
 686 2007.

687 Kulmala, M., Kontkanen, J., Junninen, H., Lehtipalo, K., Manninen, H. E., Nieminen, T., Petäjä, T., Sipilä,  
 688 M., Schobesberger, S., Rantala, P., Franchin, A., Jokinen, T., Järvinen, E., Äijälä, M., Kangasluoma, J.,  
 689 Hakala, J., Aalto, P. P., Paasonen, P., Mikkilä, J., Vanhanen, J., Aalto, J., Hakola, H., Makkonen, U.,  
 690 Ruuskanen, T., Mauldin, R. L., Duplissy, J., Vehkamäki, H., Bäck, J., Kortelainen, A., Riipinen, I., Kurtén,  
 691 T., Johnston, M. V., Smith, J. N., Ehn, M., Mentel, T. F., Lehtinen, K. E. J. J., Laaksonen, A., Kerminen, V.-  
 692 M. M. V.-M., Worsnop, D. R., Petaja, T., Sipila, M., Schobesberger, S., Rantala, P., Franchin, A., Jokinen,

693 T., Jarvinen, E., Aijala, M., Kangasluoma, J., Hakala, J., Aalto, P. P., Paasonen, P., Mikkila, J., Vanhanen, J.,  
694 Aalto, J., Hakola, H., Makkonen, U., Ruuskanen, T., Mauldin, R. L., Duplissy, J., Vehkamaki, H., Back, J.,  
695 Kortelainen, A., Riipinen, I., Kurten, T., Johnston, M. V., Smith, J. N., Ehn, M., Mentel, T. F., Lehtinen, K.,  
696 E. J. J., Laaksonen, A., Kerminen, V.-M. M. V.-M., Worsnop, D. R., Petäjä, T., Sipilä, M., Schobesberger,  
697 S., Rantala, P., Franchin, A., Jokinen, T., Järvinen, E., Äijälä, M., Kangasluoma, J., Hakala, J., Aalto, P. P.,  
698 Paasonen, P., Mikkilä, J., Vanhanen, J., Aalto, J., Hakola, H., Makkonen, U., Ruuskanen, T., Mauldin, R. L.,  
699 Duplissy, J., Vehkamäki, H., Bäck, J., Kortelainen, A., Riipinen, I., Kurtén, T., Johnston, M. V., Smith, J. N.,  
700 et al.: Direct observations of atmospheric aerosol nucleation., *Science*, 339(6122), 943–6,  
701 doi:10.1126/science.1227385, 2013.

702 Kulmala, M., Ezhova, E., Kalliokoski, T., Noe, S., Vesala, T., Lohila, A., Liski, J., Makkonen, R., Bäck, J.,  
703 Petäjä, T. and Kerminen, V.-M.: CarbonSink+-Accounting for multiple climate feedbacks from forests,  
704 *Boreal Environ. Res.*, 25, 145-159, 2020.

705 Kürten, A., Rondo, L., Ehrhart, S. and Curtius, J.: Calibration of a chemical ionization mass spectrometer for  
706 the measurement of gaseous sulfuric acid, *J. Phys. Chem. A*, 116(24), 6375–6386, doi:10.1021/jp212123n,  
707 2012.

708 Kürten, A., Jokinen, T., Simon, M., Sipilä, M., Sarnela, N., Junninen, H., Adamov, A., Almeida, J., Amorim,  
709 A., Bianchi, F., Breitenlechner, M., Dommen, J., Donahue, N. M., Duplissy, J., Ehrhart, S., Flagan, R. C.,  
710 Franchin, A., Hakala, J., Hansel, A., Heinritzi, M., Hutterli, M., Kangasluoma, J., Kirkby, J., Laaksonen, A.,  
711 Lehtipalo, K., Leiminger, M., Makhmutov, V., Mathot, S., Onnella, A., Petäjä, T., Praplan, A. P., Riccobono,  
712 F., Rissanen, M. P., Rondo, L., Schobesberger, S., Seinfeld, J. H., Steiner, G., Tomé, A., Tröstl, J., Winkler,  
713 P. M., Williamson, C., Wimmer, D., Ye, P., Baltensperger, U., Carslaw, K. S., Kulmala, M., Worsnop, D. R.,  
714 Curtius, J. and Barbara Finlayson-Pitts, by J.: Neutral molecular cluster formation of sulfuric acid–  
715 dimethylamine observed in real time under atmospheric conditions, *Proc. Natl. Acad. Sci. U.S.A.*, 111(42),  
716 15019–15024, doi:10.1073/pnas.1404853111, 2014.

717 Kyrö, E. M., Väänänen, R., Kerminen, V. M., Virkkula, A., Petäjä, T., Asmi, A., Dal Maso, M., Nieminen,  
718 T., Juhola, S., Shcherbinin, A., Riipinen, I., Lehtipalo, K., Keronen, P., Aalto, P. P., Hari, P. and Kulmala,  
719 M.: Trends in new particle formation in eastern Lapland, Finland: Effect of decreasing sulfur emissions from  
720 Kola Peninsula, *Atmos. Chem. Phys.*, 14(9), 4383–4396, 2014.

721 Lai, S. C., Williams, J., Arnold, S. R., Atlas, E. L., Gebhardt, S. and Hoffmann, T.: Iodine containing species  
722 in the remote marine boundary layer: A link to oceanic phytoplankton, *Geophys. Res. Lett.*, 38(20),  
723 doi:10.1029/2011GL049035, 2011.

724 Lehtipalo, K., Yan, C., Dada, L., Bianchi, F., Xiao, M., Wagner, R., Stolzenburg, D., Ahonen, L. R.,  
725 Amorim, A., Baccarini, A., Bauer, P. S., Baumgartner, B., Bergen, A., Bernhammer, A.-K., Breitenlechner,  
726 M., Brilke, S., Buchholz, A., Mazon, S. B., Chen, D., Chen, X., Dias, A., Dommen, J., Draper, D. C.,  
727 Duplissy, J., Ehn, M., Finkenzeller, H., Fischer, L., Frege, C., Fuchs, C., Garmash, O., Gordon, H., Hakala,  
728 J., He, X., Heikkilä, L., Heinritzi, M., Helm, J. C., Hofbauer, V., Hoyle, C. R., Jokinen, T., Kangasluoma,  
729 J., Kerminen, V.-M., Kim, C., Kirkby, J., Kontkanen, J., Kürten, A., Lawler, M. J., Mai, H., Mathot, S.,  
730 Mauldin, R. L., Molteni, U., Nichman, L., Nie, W., Nieminen, T., Ojdanic, A., Onnella, A., Passananti, M.,  
731 Petäjä, T., Piel, F., Pospisilova, V., Quéléver, L. L. J., Rissanen, M. P., Rose, C., Sarnela, N., Schallhart, S.,  
732 Schuchmann, S., Sengupta, K., Simon, M., Sipilä, M., Tauber, C., Tomé, A., Tröstl, J., Väistönen, O., Vogel,  
733 A. L., Volkamer, R., Wagner, A. C., Wang, M., Weitz, L., Wimmer, D., Ye, P., Yli-Sirniö, A., Zha, Q.,  
734 Carslaw, K. S., Curtius, J., Donahue, N. M., Flagan, R. C., Hansel, A., Riipinen, I., Virtanen, A., Winkler, P.,  
735 M., Baltensperger, U., Kulmala, M. and Worsnop, D. R.: Multicomponent new particle formation from  
736 sulfuric acid, ammonia, and biogenic vapors, *Sci. Adv.*, 4(12), eaau5363, doi:10.1126/sciadv.aau5363, 2018.

737 Leino, K., Nieminen, T., Manninen, H. E., Petäjä, T., Kerminen, V.-M. and Kulmala, M.: Intermediate ions  
738 as a strong indicator of new particle formation bursts in a boreal forest, *Boreal Environ. Res.*, 21(3-4), 274–  
739 286, 2016.

740 Levasseur, M.: Impact of Arctic meltdown on the microbial cycling of sulphur., *Nat. Geosci.*, 6(9), 691-700,  
741 2013.

742 Mäkelä, J. M., Aalto, P., Jokinen, V., Pohja, T., Nissinen, A., Palmroth, S., Markkanen, T., Seitsonen, K.,  
743 Lihavainen, H. and Kulmala, M.: Observations of ultrafine aerosol particle formation and growth in boreal  
744 forest, *Geophys. Res. Lett.*, 24(10), 1219–1222, doi:10.1029/97GL00920, 1997.

745 Manninen, H. E., Mirme, S., Mirme, A., Petäjä, T. and Kulmala, M.: How to reliably detect molecular  
746 clusters and nucleation mode particles with Neutral cluster and Air Ion Spectrometer (NAIS), *Atmos. Meas.  
747 Tech.*, 9(8), 3577–3605, 2016.

748 Maso, M. D., Dal Maso, M., Kulmala, M., Riipinen, I., Wagner, R., Hussein, T., Aalto, P. P. and Lehtinen,  
749 K. E. J.: Formation and growth of fresh atmospheric aerosols: Eight years of aerosol size distribution data  
750 from SMEAR II, Hyytiälä, Finland, *Boreal Environ. Res.*, 10(5), 323–336, 2005.

751 Mauldin, R., Kosciuch, E., Eisele, F., Huey, G., Tanner, D., Sjostedt, S., Blake, D., Chen, G., Crawford, J.  
752 and Davis, D.: South Pole Antarctica observations and modeling results: New insights on HO<sub>x</sub> radical and  
753 sulfur chemistry, *Atmos. Environ.*, 44(4), 572–581, doi:10.1016/j.atmosenv.2009.07.058, 2010.

754 Mauldin, R. L., Kosciuch, E., Henry, B., Eisele, F. L., Shetter, R., Lefer, B., Chen, G., Davis, D., Huey, G.  
755 and Tanner, D.: Measurements of OH, HO<sub>2</sub>+RO<sub>2</sub>, H<sub>2</sub>SO<sub>4</sub>, and MSA at the South Pole during ISCAT 2000,  
756 *Atmos. Environ.*, 38(32), 5423–5437, doi:10.1016/j.atmosenv.2004.06.031, 2004.

757 McFiggans, G., Bale, C. S. E. E., Ball, S. M., Beames, J. M., Bloss, W. J., Carpenter, L. J., Dorsey, J., Dunk,  
758 R., Flynn, M. J., Furneaux, K. L., Gallagher, M. W., Heard, D. E., Hollingsworth, A. M., Hornsby, K.,  
759 Ingham, T., Jones, C. E., Jones, R. L., Kramer, L. J., Langridge, J. M., Leblanc, C., LeCrane, J. P.-P., Lee, J.  
760 D., Leigh, R. J., Longley, I., Mahajan, A. S., Monks, P. S., Oetjen, H., Orr-Ewing, a. J., Plane, J. M. C. C.,  
761 Potin, P., Shillings, a. J. L. L., Thomas, F., Von Glasow, R., Wada, R., Whalley, L. K. and Whitehead, J. D.:  
762 Iodine-mediated coastal particle formation: an overview of the Reactive Halogens in the Marine Boundary  
763 Layer (RHAMBLe) Roscoff coastal study, *Atmos. Chem. Phys.*, 10(6), 2975–2999, doi:10.5194/acpd-9-  
764 26421-2009, 2010.

765 Mirme, S. and Mirme, A.: The mathematical principles and design of the NAIS – a spectrometer for the  
766 measurement of cluster ion and nanometer aerosol size distributions, *Atmos. Meas. Tech.*, 6(4), 1061–1071,  
767 doi:10.5194/amt-6-1061-2013, 2013.

768 Myllys, N., Ponkkonen, T., Passananti, M., Elm, J., Vehkämäki, H. and Olenius, T.: Guanidine: A Highly  
769 Efficient Stabilizer in Atmospheric New-Particle Formation, *J. Phys. Chem. A*, 122(20), 4717–4729,  
770 doi:10.1021/acs.jpca.8b02507, 2018.

771 Napari, I., Noppel, M., Vehkämäki, H. and Kulmala, M.: Parametrization of ternary nucleation rates for  
772 H<sub>2</sub>SO<sub>4</sub>-NH<sub>3</sub>-H<sub>2</sub>O vapors, *J. Geophys. Res. Atmos.*, 107(19), AAC 6-1-AAC 6-6,  
773 doi:10.1029/2002JD002132, 2002.

774 Nieminen, T., Asmi, A., Maso, M. D., Aalto, P. P., Keronen, P., Kulmala, M., Kerminen, V., Dal maso, M.,  
775 Aalto, P. P., Keronen, P., Petäjä, T., Kulmala, M. and Kerminen, V.: Trends in atmospheric new-particle  
776 formation: 16 years of observations in a boreal-forest environment, *Boreal Environ. Res.*, 19 (suppl.(2004)),  
777 191–214, 2014.

778 O'Dowd, C. D., Jimenez, J. L., Bahreini, R., Flagan, R. C., Seinfeld, J. H., Hämerl, K., Pirjola, L., Kulmala,  
779 M. and Hoffmann, T.: Marine aerosol formation from biogenic iodine emissions, *Nature*, 417(6889), 632–  
780 636, 2002.

781 Paasonen, P., Asmi, A., Petäjä, T., Kajos, M. K., Äijälä, M., Junninen, H., Holst, T., Abbatt, J. P. D. D.,  
782 Arnett, A., Birmili, W., Van Der Gon, H. D., Hamed, A., Hoffer, A., Laakso, L., Laaksonen, A., Richard  
783 Leaitch, W., Plass-Dülmer, C., Pryor, S. C., Räisänen, P., Swietlicki, E., Wiedensohler, A., Worsnop, D. R.,  
784 Kerminen, V.-M. M. and Kulmala, M.: Warming-induced increase in aerosol number concentration likely to  
785 moderate climate change, *Nat. Geosci.*, 6(6), 438–442, doi:10.1038/ngeo1800, 2013.

786 Park, K., Lee, K., Kim, T., Yoon, Y. J., Jang, E., Jang, S., Lee, B. and Hermansen, O.: Atmospheric DMS in  
787 the Arctic Ocean and Its Relation to Phytoplankton Biomass, *Global Biogeochem. Cycles*, 32(3), 351–359,  
788 doi:10.1002/2017GB005805, 2018.

789 Pirjola, L., Laaksonen, A., Aalto, P. and Kulmala, M.: Sulfate aerosol formation in the Arctic boundary  
790 layer, *J. Geophys. Res. Atmos.*, 103(D7), 8309–8321, doi:10.1029/97JD03079, 1998.

791 Raso, A. R. W., Custard, K. D., May, N. W., Tanner, D., Newburn, M. K., Walker, L., Moore, R. J., Huey,  
792 L. G., Alexander, L., Shepson, P. B. and Pratt, K. A.: Active molecular iodine photochemistry in the Arctic,  
793 *Proc. Natl. Acad. Sci. U. S. A.*, 114(38), 10053–10058, doi:10.1073/pnas.1702803114, 2017.

794 Reyer, C. P. O., Brouwers, N., Rammig, A., Brook, B. W., Epila, J., Grant, R. F., Holmgren, M.,  
795 Langerwisch, F., Leuzinger, S., Lucht, W., Medlyn, B., Pfeifer, M., Steinkamp, J., Vanderwel, M. C.,  
796 Verbeeck, H. and Villela, D. M.: Forest resilience and tipping points at different spatio-temporal scales:  
797 Approaches and challenges, *J. Ecol.*, 103(1), 5–15, doi:10.1111/1365-2745.12337, 2015.

798 Riva, M., Rantala, P., Krechmer, E. J., Peräkylä, O., Zhang, Y., Heikkinen, L., Garmash, O., Yan, C.,  
799 Kulmala, M., Worsnop, D. and Ehn, M.: Evaluating the performance of five different chemical ionization  
800 techniques for detecting gaseous oxygenated organic species, *Atmos. Meas. Tech.*, 12(4), 2403–2421,  
801 doi:10.5194/amt-12-2403-2019, 2019.

802 Ruuskanen, T., Reissell, M., Keronen, A., Aalto, P. P., Laakso, P. P., Grönholm, L., Hari, T. and Kulmala,  
803 P.: Atmospheric trace gas and aerosol particle concentration measurements in Eastern Lapland, *Boreal Env.*  
804 *Res.*, 8(4), 335–349, 2003.

805 Ruuskanen, T. M., Kaasik, M., Aalto, P. P., Hörrak, U., Vana, M., Mårtensson, M., Yoon, Y. J., Keronen, P.,  
806 Mordas, G., Ceburnis, D., Nilsson, E. D., O'Dowd, C., Noppel, M., Alliksaar, T., Ivask, J., Sofiev, M.,  
807 Prank, M. and Kulmala, M.: Concentrations and fluxes of aerosol particles during the LAPBIAT  
808 measurement campaign at Väriö field station, *Atmos. Chem. Phys.*, 7(14), 3683–3700, doi:10.5194/acp-7-  
809 3683-2007, 2007.

810 Schmale, J., Zieger, P. and Ekman, A. M. L.: Aerosols in current and future Arctic climate, *Nat. Clim.*  
811 Chang., 11(2), 95–105, doi:10.1038/s41558-020-00969-5, 2021.

812 Seco, R., Holst, T., Sillesen Matzen, M., Westergaard-Nielsen, A., Li, T., Simin, T., Jansen, J., Crill, P.,  
813 Friborg, T., Rinne, J. and Rinnan, R.: Volatile organic compound fluxes in a subarctic peatland and lake,  
814 *Atmos. Chem. Phys.*, 20(21), 13399–13416, doi:10.5194/ACP-20-13399-2020, 2020.

815 Sherwen, T. M., Evans, M. J., Spracklen, D. V., Carpenter, L. J., Chance, R., Baker, A. R., Schmidt, J. A.  
816 and Breider, T. J.: Global modeling of tropospheric iodine aerosol, *Geophys. Res. Lett.*, 43(18), 10012–  
817 10019, doi:10.1002/2016gl070062, 2016.

818 Sipilä, M., Sarnela, N., Jokinen, T., Henschel, H., Junninen, H., Kontkanen, J., Richters, S., Kangasluoma, J.,  
819 Franchin, A., Peräkylä, O., Rissanen, M. P., Ehn, M., Vehkamäki, H., Kurten, T., Berndt, T., Petäjä, T.,  
820 Worsnop, D., Ceburnis, D., Kerminen, V.-M. M., Kulmala, M., O'Dowd, C. and O'Dowd, C.: Molecular-  
821 scale evidence of aerosol particle formation via sequential addition of  $\text{HIO}_3$ , *Nature*, 537(7621), 532–534,  
822 doi:10.1038/nature19314, 2016.

823 Sipilä, M., Sarnela, N., Neitola, K., Laitinen, T., Kemppainen, D., Beck, L., Duplissy, E.-M., Kuittinen, S.,  
824 Lehtusjärvi, T., Lampilahti, J., Kerminen, V.-M., Lehtipalo, K., Aalto, P., Keronen, P., Siivola, E., Rantala,  
825 P., Worsnop, D., Kulmala, M., Jokinen, T. and Petäjä, T.: Wintertime sub-arctic new particle formation from  
826 Kola Peninsula sulphur emissions, *Atmos. Chem. Phys.*, 21(23), 17559–17576,  
827 doi:<https://doi.org/10.5194/acp-21-17559-2021>, 2021.

828 Sive, B. C., Varner, R. K., Mao, H., Blake, D. R., Wingenter, O. W. and Talbot, R.: A large terrestrial source  
829 of methyl iodide, *Geophys. Res. Lett.*, 34(17), L17808, doi:10.1029/2007gl030528, 2007.

830 Spolaor, A., Barbaro, E., Cappelletti, D., Turetta, C., Mazzola, M., Giardi, F., Björkman, M., Lucchetta, F.,  
831 Dallo, F., Pfaffhuber, K. A., Angot, H., Dommergue, A., Maturilli, M., Saiz-Lopez, A., Barbante, C. and  
832 Cairns, W.: Diurnal cycle of iodine and mercury concentrations in Svalbard surface snow, *Atmos. Chem.*  
833 *Phys. Discuss.*, 1–25, doi:10.5194/ACP-2019-285, 2019.

834 Stohl, A.: Characteristics of atmospheric transport into the Arctic troposphere, *J. Geophys. Res. Atmos.*, 111,  
835 D11306, doi:10.1029/2005JD006888, 2006.

836 Sulo, J., Sarnela, N., Kontkanen, J., Ahonen, L., Paasonen, P., Laurila, T., Jokinen, T., Kangasluoma, J.,  
837 Junninen, H., Sipilä, M., Petäjä, T., Kulmala, M. and Lehtipalo, K.: Long-term measurement of sub-  
838 3&thinsp;nm particles and their precursor gases in the boreal forest, *Atmos. Chem. Phys.*, 21(2), 695–715,  
839 doi:10.5194/acp-21-695-2021, 2021.

840 Tarvainen, V., Hakola, H., Hellén, H., Bäck, J., Hari, P. and Kulmala, M.: Temperature and light dependence  
841 of the VOC emissions of Scots pine, *Atmos. Chem. Phys.*, 4(5), 989–998, doi: 10.5194/acp-5-989-2005,  
842 2004.

843 Tiiva, P., Faubert, P., Michelsen, A., Holopainen, T., Holopainen, J. K. and Rinnan, R.: Climatic warming  
844 increases isoprene emission from a subarctic heath, *New Phytol.*, 180(4), 853–863, doi:10.1111/j.1469-  
845 8137.2008.02587.X, 2008.

846 Tunved, P., Hansson, H. C., Kerminen, V. M., Ström, J., Dal Maso, M., Lihavainen, H., Viisanen, Y., Aalto,  
847 P. P., Komppula, M. and Kulmala, M.: High natural aerosol loading over boreal forests, *Science* (80-..),  
848 312(5771), 261–263, doi:10.1126/science.1123052, 2006.

849 Valolahti, H., Kivimäenpää, M., Faubert, P., Michelsen, A. and Rinnan, R.: Climate change-induced  
850 vegetation change as a driver of increased subarctic biogenic volatile organic compound emissions, *Glob.*  
851 *Chang. Biol.*, 21(9), 3478–3488, doi:10.1111/GCB.12953, 2015.

852 Vana, M., Komsaare, K., Hörrak, U., Mirme, S., Nieminen, T., Kontkanen, J., Manninen, H. E., Petäjä, T.,  
853 Noe, S. M. and Kulmala, M.: Characteristics of new-particle formation at three SMEAR stations, *Boreal*  
854 *Environ. Res.*, 21(3-4), 345–362, 2016.

855 Vehkamäki, H., Dal Maso, M., Hussein, T., Flanagan, R., Hyvärinen, A., Lauros, J., Merikanto, J.,  
856 Mönkkönen, P., Pihlatie, M., Salminen, K., Sogacheva, L., Thum, T., Ruuskanen, T. M., Keronen, P., Aalto,  
857 P. P., Hari, P., Lehtinen, K. E. J., Rannik, Ü. and Kulmala, M.: Atmospheric particle formation events at  
858 Väriö measurement station in Finnish Lapland 1998–2002, *Atmos. Chem. Phys.*, 4(7), 2015–2023,  
859 doi:10.5194/acp-4-2015-2004, 2004.

860 Wang, S., Riva, M., Yan, C., Ehn, M. and Wang, L.: Primary Formation of Highly Oxidized Multifunctional  
861 Products in the OH-Initiated Oxidation of Isoprene: A Combined Theoretical and Experimental Study,  
862 *Environ. Sci. Technol.*, 52(21), 12255–12264, doi:10.1021/acs.est.8b02783, 2018.

863 Wang, Y. Q., Zhang, X. Y. and Draxler, R. R.: TrajStat: GIS-based software that uses various trajectory  
864 statistical analysis methods to identify potential sources from long-term air pollution measurement data,  
865 *Environ. Model. Softw.*, 24(8), 938–939, doi:10.1016/j.envsoft.2009.01.004, 2009.

866 Yan, C., Nie, W., Äijälä, M., Rissanen, M. P., Canagaratna, M. R., Massoli, P., Junninen, H., Jokinen, T.,  
867 Sarnela, N., Häme, S. A. K. K., Schobesberger, S., Canonaco, F., Yao, L., Prévôt, A. S. H. H., Petäjä, T.,  
868 Kulmala, M., Sipilä, M., Worsnop, D. R., Ehn, M., Äijälä, M., Rissanen, M. P., Canagaratna, M. R., Massoli,  
869 P., Junninen, H., Jokinen, T., Sarnela, N., Häme, S. A. K. K., Schobesberger, S., Canonaco, F., Yao, L.,  
870 Prévôt, A. S. H. H., Petäjä, T., Kulmala, M., Sipilä, M., Worsnop, D. R. and Ehn, M.: Source  
871 characterization of highly oxidized multifunctional compounds in a boreal forest environment using positive  
872 matrix factorization, *Atmos. Chem. Phys.*, 16(19), 12715–12731, doi:10.5194/acp-16-12715-2016, 2016.

873 Yu, H., Ren, L., Huang, X., Xie, M., He, J. and Xiao, H.: Iodine speciation and size distribution in ambient  
874 aerosols at a coastal new particle formation hotspot in China, *Atmos. Chem. Phys.*, 19(6), 4025–4039,  
875 doi:10.5194/acp-19-4025-2019, 2019.

876